

# Lectures on Dark Energy and Cosmic Acceleration

Joshua A. Frieman

*Fermilab Center for Particle Astrophysics, Batavia, IL 60510  
Kavli Institute for Cosmological Physics, The University of Chicago, Chicago, IL 60637*

**Abstract.** The discovery ten years ago that the expansion of the Universe is accelerating put in place the present cosmological model, in which the Universe is composed of 4% baryons, 20% dark matter, and 76% dark energy. Yet the underlying cause of cosmic acceleration remains a mystery: it could arise from the repulsive gravity of dark energy – for example, the quantum energy of the vacuum – or it may signal that General Relativity breaks down on cosmological scales and must be replaced. In these lectures, I present the observational evidence for cosmic acceleration and what it has revealed about dark energy, discuss a few of the theoretical ideas that have been proposed to explain acceleration, and describe the key observational probes that we hope will shed light on this enigma in the coming years. Based on five lectures given at the XII Ciclo de Cursos Especiais at the Observatorio Nacional, Rio de Janeiro, Brazil, 1-5 October 2007.

**Keywords:** dark energy – cosmic acceleration

## INTRODUCTION

In 1998, two teams studying distant Type Ia supernovae presented independent evidence that the expansion of the Universe is speeding up [1, 2]. Subsequent observations, including more detailed studies of supernovae and independent evidence from the cosmic microwave background, large-scale structure, and clusters of galaxies, have confirmed and firmly established this remarkable finding. These lectures<sup>1</sup> provide a short pedagogical overview of dark energy, including: 1. A brief review of cosmology; 2. The discovery of cosmic acceleration from observations of distant supernovae, followed by measurements of the cosmic microwave background and of baryon acoustic oscillations (BAO) in large-scale galaxy clustering; 3. The current status of the evidence for cosmic acceleration; 4. Theories of acceleration, including dark energy, the cosmological constant, and modified gravity; 5. Probes of dark energy, including clusters and weak gravitational lensing in addition to supernovae and BAO; and 6. A summary of current and future projects aimed at probing acceleration through the history of cosmic expansion and the growth of large-scale structure.

A number of useful reviews target different aspects of the subject, including: theory [3, 4]; cosmology [5]; the physics of cosmic acceleration [6]; probes of dark energy [7]; dark energy reconstruction [8]; dynamics of dark energy models [9]; the cosmological constant [10, 11], and the cosmological constant problem [12]. These lecture notes most

---

<sup>1</sup> The slides of the lectures are available at <http://www.on.br/institucional/portuguese/dppg/cpgastron/ciclo2007/lectures.html>.

closely follow (and borrow from) the recent review of Frieman et al. [13].

## BRIEF REVIEW OF COSMOLOGY

The Friedmann-Robertson-Walker (FRW) cosmological model provides the context for interpreting the observational evidence for cosmic acceleration as well as the framework for understanding how cosmological probes in the future will help uncover the cause of acceleration. For further details on basic cosmology, see, e.g., the textbooks of Dodelson [14], Kolb and Turner [15], Peacock [16], and Peebles [17].

The Universe is filled with a bath of thermal radiation, the cosmic microwave background radiation (CMB). The CMB has a purely thermal spectrum to the precision with which it has been measured so far, with a temperature of  $T = 2.725$  K above absolute zero. On all angular scales, it is observed to be nearly isotropic (rotationally invariant) around us, with temperature fluctuations on the order of  $\delta T/T \sim 10^{-5}$ . CMB photons have been travelling freely since the epoch of *last scattering*, when ionized plasma (re)combined to form neutral hydrogen, around 380,000 years after the Big Bang. To first approximation, maps of the CMB give us a picture of conditions at this early time and show that the young Universe was quite smooth.

According to the *Cosmological Principle*, also called the Copernican Principle, we are not privileged observers. Therefore, the Universe should appear quasi-isotropic, when averaged over large scales, to all similar observers. (Here, similar observers are those moving slowly with respect to the comoving coordinates introduced below.) A Universe that appears isotropic to all such observers can be shown to be *homogeneous*, that is, essentially the same at every location, again averaged over large scales. More specifically, the density of the cosmic fluid, when averaged over scales larger than  $\sim 100$  Mpc, is approximately translation-invariant.

## The Expanding Universe

The only time-dependent degree of freedom which preserves homogeneity and isotropy is overall expansion or contraction. Preservation of this high degree of symmetry implies that the Universe on the largest scales is described by a single degree of freedom, the cosmic scale factor,  $a(t)$ , where  $t$  is cosmic time. The spatial hypersurfaces at fixed time can be described in terms of expanding or comoving coordinates, much like the points of constant longitude and latitude on an expanding spherical balloon. To first approximation, i.e., neglecting small peculiar velocities, galaxies are at rest in these comoving coordinates, and the scale factor describes the time dependence of their physical separations,  $d = a(t)r$ , where  $r$  is the fixed comoving distance between them. Comparing the physical separations at times  $t_1$  and  $t_2$ , the apparent recession speed is given by

$$v = \frac{d(t_2) - d(t_1)}{t_2 - t_1} = \frac{r[a(t_2) - a(t_1)]}{t_2 - t_1} = \frac{d}{a} \frac{da}{dt} \equiv dH(t) \simeq dH_0, \quad (1)$$

where  $H(t) \equiv (1/a)(da/dt) = \dot{a}/a$  is the expansion rate,  $H_0$  is the Hubble parameter, the present value of  $H(t)$ , and the final equality in Eqn.1 holds for small time intervals,  $t_2 - t_1 \ll 1/H_0$ . We use the subscript '0' on a quantity to denote its value at the present epoch.

The physical wavelengths of radiation scale with the scale factor,  $\lambda \sim a(t)$ . As a result, in an expanding Universe, light emitted by one observer at time  $t_1$  and observed by another at a later time  $t_2$  is observed to be shifted to longer, redder wavelengths. The redshift  $z$  is thus defined by

$$1 + z = \frac{\lambda(t_2)}{\lambda(t_1)} = \frac{a(t_2)}{a(t_1)}, \quad (2)$$

and directly yields the relative size of the Universe at the time of emission. For nearby galaxies, the redshift is related to the apparent recession velocity by  $z \simeq v/c$ . In optical surveys, more distant galaxies have their light shifted farther to the red: they emitted their light when the Universe was smaller, indicating that it has been expanding.

In the early 1920's, Slipher reported spectroscopic measurements of recession velocities for 40 relatively nearby spiral galaxies. In the late 1920's, Hubble found Cepheid variable stars in  $\sim 20$  nearby galaxies and measured their periods of variability. Using the period-luminosity correlation previously found by Henrietta Leavitt for Galactic Cepheids, he was able to infer their luminosities. From measurements of their apparent brightnesses, he could thus deduce their distances. Comparing these distances with Slipher's radial velocities, Hubble found empirically that  $v = H_0 d$ , in agreement with the prediction for an expanding universe (Eqn. 1). While Hubble's measurements were confined to the relatively local universe,  $d \sim \text{few Mpc}$ , where peculiar velocities due to large-scale structure, of order 300 km/sec, are comparable to the expansion velocity, modern observations have extended the measurement to much larger distances. The Hubble Space Telescope Key Project used measurements to  $d \sim 300$  Mpc and found  $H_0 = 72 \pm 8$  km/s/Mpc [18].

## Expansion Dynamics

How does the expansion of the Universe change over time? Since gravity dominates over other forces on the largest scales, one expects that mutual gravitational attraction of the matter in the Universe would lead to a slowing of the expansion over time. We can put more meat (preferably churrasco) on this statement by considering cosmological dynamics.

A Newtonian treatment captures the essence of the argument. Consider a test mass  $m$  a distance  $d$  from the center of a homogeneous, spherical ball of matter that we imagine carving out from the Universe. The total mass of the ball is  $M = (4\pi/3)\rho d^3$ , where  $\rho$  is the density of the Universe. By Newton's theorem, the total energy of the test mass is given by

$$E = \frac{mv^2}{2} - \frac{GMm}{d}, \quad (3)$$

and is conserved. Using Hubble's law,  $v = Hd$ , we find the Friedmann equation,

$$\frac{2E}{md^2} \equiv -\frac{K}{a^2(t)} = H^2(t) - \left(\frac{8\pi}{3}\right) G\rho(t), \quad (4)$$

where  $K$  is a constant. In General Relativity,  $K$  emerges as the indicator of the global spatial curvature of constant-time hypersurfaces:  $K = 0$  for flat, Euclidean space,  $K > 0$  for positively curved, spherical geometry, and  $K < 0$  for a negatively curved, three-dimensional hyperboloid or saddle.

The full General Relativistic Friedmann equations for a multi-component Universe can be written

$$H^2(t) \equiv \left(\frac{1}{a} \frac{da}{dt}\right)^2 = \frac{8\pi G}{3} \sum_i \rho_i(t) - \frac{k}{a^2(t)}, \quad (5)$$

where  $k = 0, +1, -1$  for zero, positive, and negative curvature, and

$$\frac{1}{a} \frac{d^2a}{dt^2} = -\frac{4\pi G}{3} \sum_i (\rho_i + 3p_i), \quad (6)$$

where  $p_i$  and  $\rho_i$  are the pressure and density of the  $i$ th component. From Eqn. 5, it is convenient to define the critical density for a spatially flat Universe,  $\rho_{crit} \equiv 3H_0^2/8\pi G = 1.88h^2 \times 10^{-29} \text{ gm/cm}^3$ , where the dimensionless Hubble parameter  $h = H_0/(100 \text{ km/sec/Mpc})$ . The present density parameter in the  $i$ th component is then  $\Omega_{i,0} = \rho_i(t_0)/\rho_{crit}$ .

The Einstein equations also imply conservation of stress-energy, which takes the form

$$\frac{d\rho_i}{dt} + 3(\rho_i + p_i)H = 0. \quad (7)$$

If the pressure and energy density are related by  $p_i = w_i\rho_i$ , then the density in the  $i$ th component scales as

$$\rho_i \propto \exp \left[ 3 \int_0^z [1 + w_i(z')] d \ln(1 + z') \right]. \quad (8)$$

If the equation of state parameter  $w_i$  is time-independent, then

$$\rho_i \sim a^{-3(1+w_i)}. \quad (9)$$

For non-relativistic matter,  $w_m \sim (v_m/c)^2 \ll 1$ , and  $\rho_m \sim a^{-3}$ ; for radiation or more generally for ultra-relativistic particles,  $w_r = 1/3$ , and  $\rho_r \sim a^{-4}$ . Currently,  $\Omega_m \simeq 0.25$  and  $\Omega_r \simeq 0.8 \times 10^{-4}$ , implying that the Universe was radiation-dominated at epochs for which  $1 + z > a(t_0)/a(t_{eq}) \simeq 3000$ .

For much of the 1980's and 90's, a burning question was whether the Universe would expand forever or recollapse. For a matter-dominated universe,  $w_{tot} = w_m \simeq 0$ , "geometry is destiny": from Eq. 5, positive curvature, i.e.,  $k > 0$ , implies  $\Omega_{m,0} > 1$ , and since  $\rho_m$  drops more rapidly than the spatial curvature term as  $a(t)$  becomes large, the Universe reaches a maximum size ( $H = 0$ ) and subsequently recollapses. If  $k \leq 0$ , then

$\Omega_{m,0} \leq 1$ , and  $H(t)$  remains positive: the Universe expands forever. Moreover, from Eqn. 6 we have  $\ddot{a} < 0$  in all cases: the expansion of the Universe decelerates due to gravity, as one expects.

## Cosmic Acceleration and Dark Energy

In 1998, two groups observing distant supernovae found evidence that the expansion of the Universe is instead speeding up,  $\ddot{a} > 0$  [1, 2]. Since then, evidence has accumulated that the Universe was decelerating at early times but began accelerating about five billion years ago. Logically, there are three possible modes of explanation for this behavior: (i) we posit a form of “gravitationally repulsive” stress-energy in the Universe, now called Dark Energy, which came to dominate over non-relativistic matter about 5 billion years ago; (ii) we instead modify the geometric as opposed to the stress-tensor components of the Einstein-Hilbert action of General Relativity, a modification primarily manifest only on cosmologically large scales; (iii) we leave General Relativity and the matter-dominated Universe intact and instead drop the assumption that the Universe is spatially homogeneous on large scales, invoking large-scale structure to induce an apparent acceleration. Either of the first two would have profound implications for our understanding of fundamental physics. We will return to some of these theoretical ideas in a later chapter.

Dark energy is perhaps the simplest explanation for cosmic acceleration and the most familiar. From Eqs. 6 and 9, if a component has an equation of state parameter  $w < -1/3$ , i.e., sufficiently negative pressure, then it will come to dominate over other forms of stress-energy and will drive accelerated expansion. This is the defining property of dark energy. An immediate consequence is that the link between geometry and destiny is broken: for example, while  $\Omega_0 > 1$  still implies positive spatial curvature,  $k > 0$ , it does not mean that the Universe will necessarily recollapse, because the dark energy density scales more slowly with  $a(t)$  than the spatial curvature term, which goes as  $1/a^2(t)$ . The FRW scale factor vs. time is shown in Fig. 1a for various cosmological parameter choices. The history of the matter, radiation, and dark energy components is shown in Fig. 1b.

The simplest candidate for dark energy is the cosmological constant,  $\Lambda$ . It was introduced by Einstein into the equations of General Relativity in order to produce a static, finite Universe:

$$G_{\mu\nu} - \Lambda g_{\mu\nu} = \frac{8\pi G}{c^4} T_{\mu\nu} \quad (10)$$

where  $G_{\mu\nu}$  is the Einstein tensor describing the curvature of spacetime, and  $T_{\mu\nu}$  is the stress-energy tensor of the components. When the expansion of the Universe was discovered by Hubble, Einstein advocated abandoning the cosmological constant as an unnecessary blemish on his theory. However, in the late 1960’s, Zel’dovich stressed that  $\Lambda$  logically belongs on the right-hand side of the Einstein equations, as the stress-energy of the vacuum,  $T_{\mu\nu}^{vac} = (\Lambda/8\pi G)g_{\mu\nu}$  [19]. (This point was made earlier by Lemaitre as well.) Since the vacuum energy density gets contributions from quantum zero-point fluctuations of all fields, it cannot simply be dismissed. The pressure and energy density

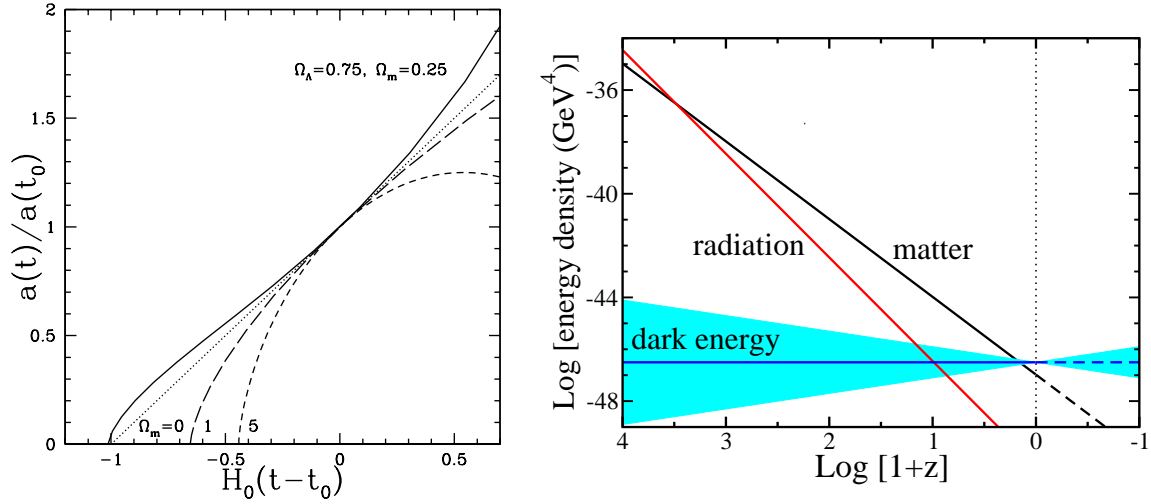


**FIGURE 1.** Left panel (a): Evolution of the scale factor vs. time for four cosmological models: three matter-dominated models with  $\Omega_0 = \Omega_m = 0, 1, 5$ , and one with  $\Omega_\Lambda = 0.75, \Omega_m = 0.25$ . Right panel (b): Evolution of radiation, matter, and dark energy densities with redshift. For dark energy, the band represents  $w = -1 \pm 0.2$ . From Frieman et al. [13].

of the vacuum can be read off from the stress-tensor as  $p_{vac} = -\rho_{vac} = \Lambda/8\pi G$ , so it acts as a fluid with equation of state parameter  $w = -1$ , as needed to explain acceleration. In a  $\Lambda$ -dominated model, the expansion is asymptotically exponential,  $a(t) \sim \exp(\sqrt{\Lambda/3}t)$ . The one fly in the ointment is that the required energy density for cosmic acceleration is of order  $\rho_{vac} \simeq (0.003 \text{ eV})^4$ , while estimates of the vacuum energy density of quantum fields are at least 60 to 120 orders of magnitude larger. This embarrassing discrepancy, which predates and is logically separate from but is brought into focus by cosmic acceleration, is known as the cosmological constant problem.

While the discovery of cosmic acceleration is often portrayed as a surprise, in fact it fit neatly into a pre-existing theoretical and observational framework that had been solidifying throughout the 1990's. There were several elements of this framework: (1) the theory of primordial inflation [20] predicted a flat Universe,  $\Omega_0 = 1$ , while observations of dark matter were pointing with increasing accuracy to  $\Omega_m \simeq 0.25$ , so a component of “missing energy” with  $\Omega_{ME} \simeq 0.75$  was needed to reconcile the two; (2) such a missing energy component must be smoothly distributed and would therefore inhibit the growth of large-scale structure—it must therefore have come to dominate over non-relativistic matter at recent cosmic epochs, which means it must have a sufficiently negative equation of state parameter,  $w \leq -0.5$ ; (3) the model of structure formation with cold dark matter and a cosmological constant,  $\Lambda$ CDM, in combination with primordial perturbations from inflation, had been found to be in good agreement with observations of the large-scale clustering of galaxies, e.g., as observed in the APM survey [21]; (4) estimates of globular cluster ages, in combination with Hubble parameter measurements, indicated that  $H_0 t_0 = (H_0/70 \text{ km/s/Mpc})(t_0/14 \text{ Gyr}) \simeq 1$  or larger, which requires an epoch during which  $a(t)$  grows as fast or faster than  $t$ , i.e., accelerated expansion (see Fig. 1a). As a result of this combination of factors, by the mid-1990's, a model

with a dominant form of dark energy was recognized as a good match to much of the cosmological data [22, 23, 24].

On the other hand, the cosmological constant had a troubled history in the 20th century. Beginning with Einstein, it had been introduced to explain apparent observations that subsequently either evaporated or were explained on other grounds. These episodes included the preponderance of quasars around  $z \sim 2$  in the late 1960's and the Hubble diagram of brightest-cluster elliptical galaxies in the mid-70's. Based on this history, healthy early skepticism of the supernova results was warranted. However, we now have independent, robust lines of evidence for cosmic acceleration from multiple sources: type Ia supernovae, the cosmic microwave background, and large-scale structure, among others. Moreover, as new data has accumulated, the evidence has strengthened.

## THE DISCOVERY OF COSMIC ACCELERATION

In this section we overview the evidence for the accelerating Universe that accrued in the late 1990's and early 2000's.

### Type Ia Supernovae

Supernovae were first studied systematically by Zwicky and collaborators in the 1930's. It was soon recognized that these luminous outbursts can be classified into different types based on their light curves and optical spectra. Type I supernovae were observed to exhibit similar light curves to each other and displayed no hydrogen in their spectra. Type II supernovae, identified by their strong hydrogen lines, showed much larger variability in their light curves. Type I supernovae were later subclassified into type Ia, which show silicon lines, type Ib, which show helium and no silicon, and type Ic, which show neither.

Although this classification is purely empirical, the type Ia supernovae appear to be a physically distinct class from the other supernova types. SNe Ia are the thermonuclear explosions of white dwarf stars that are accreting mass from a binary companion and approaching the Chandrasekhar mass. The other supernova types arise from the core collapse of evolved massive stars.

Type Ia supernovae appear quite homogeneous in their observational properties: they show similar spectral features, rise times of 15 to 20 days, and decay times of months. SN Ia light curves are powered by the radioactive decays of  $^{56}\text{Ni}$  (at early times) and  $^{56}\text{Co}$  (after a few weeks), produced in the thermonuclear explosion [25]. The peak luminosity is determined primarily by the mass of  $^{56}\text{Ni}$  produced in the explosion [26]: if the white dwarf is fully burned, one expects  $\sim 0.6M_{\odot}$  of  $^{56}\text{Ni}$  to be produced. As a result, although the detailed mechanism of SN Ia explosions remains uncertain [e.g., 27, 28], SNe Ia are expected and observed to have similar peak luminosities.

In fact, SNe Ia are not precisely standard candles, with a  $1\sigma$  spread of order 0.3 mag in peak  $B$ -band luminosity. However, work in the early 1990's [29] established an empirical correlation between SN Ia peak brightness and the rate at which the luminosity declines with time after peak: intrinsically brighter SNe Ia decline more slowly. After

correcting for this correlation, SNe Ia turn out to be excellent “standardizable” candles, with a dispersion of about 15% in peak brightness.

To put the supernova observations in context, we pause to review how distances are defined and measured in cosmology.

### *Cosmological Distances*

The spacetime metric for the homogeneous, isotropic FRW cosmology can be written in either of two useful forms:

$$\begin{aligned} ds^2 &= c^2 dt^2 - a^2(t) \left[ dr^2 / (1 - kr^2) + r^2 (d\theta^2 + \sin^2 \theta d\phi^2) \right] \\ &= c^2 dt^2 - a^2(t) \left[ d\chi^2 + S_k^2(\chi) (d\theta^2 + \sin^2 \theta d\phi^2) \right], \end{aligned} \quad (11)$$

where  $k$  is the spatial curvature index,  $\theta$ ,  $\phi$  are the usual angular coordinates in a spherical coordinate system, and  $r = S_k(\chi) = \sinh(\chi), \chi, \sin(\chi)$  for  $k = -1, 0, +1$ . Along a radial null geodesic (light ray),  $ds^2 = d\theta^2 = d\phi^2 = 0$ , so  $cdt = ad\chi$ . As a result, the comoving distance is given by

$$\chi = \int \frac{cdt}{a} = \int \frac{cdt}{ada} da = c \int \frac{da}{a^2 H(a)}. \quad (12)$$

Without loss of generality we can set  $a(t_0) \equiv a_0 = 1$ , so that  $a = 1/(1+z)$ , and we have  $da = -(1+z)^{-2} dz = -a^2 dz$ . We therefore derive a simple relation between redshift and comoving distance,  $cdz = -H(z)d\chi$ .

To compute the *luminosity distance*, consider a source  $S$  at the origin emitting light at time  $t_1$  into solid angle  $d\Omega$  that is received by observer  $O$  at coordinate distance  $r$  at time  $t_0$  who has a detector of area  $A$ . The proper area of the detector is given by the FRW metric,  $A = a_0 r d\theta a_0 r \sin \theta d\phi = a_0^2 r^2 d\Omega$ . A unit-area detector at  $O$  thus subtends a solid angle  $d\Omega = 1/a_0^2 r^2$  at  $S$ . The power emitted into  $d\Omega$  by a source of luminosity  $L$  is  $dP = Ld\Omega/4\pi$ , and the energy flux received by  $O$  per unit area is thus  $f = Ld\Omega/4\pi = L/4\pi a_0^2 r^2$ . However, the expansion of the Universe reduces the received flux due to two effects: (i) the photon energy redshifts,  $E_\gamma(t_0) = E_\gamma(t_1)/(1+z)$ ; (ii) photons emitted at time intervals  $\delta t_1$  arrive at larger time intervals given by  $\delta t_0/\delta t_1 = a(t_0)/a(t_1) = 1+z$ : this time dilation factor can be derived from the constancy of the comoving distance of Eqn. 12, i.e., by setting  $\int_{t_1}^{t_0} dt/a(t) = \int_{t_1+\delta t_1}^{t_0+\delta t_0} dt/a(t)$  and rewriting the integration limits. Including these two factors, we can write the flux as

$$f = \frac{Ld\Omega}{4\pi} = \frac{L}{4\pi a_0^2 r^2 (1+z)^2} \equiv \frac{L}{4\pi d_L^2}, \quad (13)$$

where the last equality defines the luminosity distance  $d_L$  in terms of the usual inverse-square law,

$$d_L = r(1+z) = c(1+z) |\Omega_k|^{-1/2} S_k \left( \int |\Omega_k|^{1/2} \frac{da}{H_0 a^2 (H(a)/H_0)} \right), \quad (14)$$



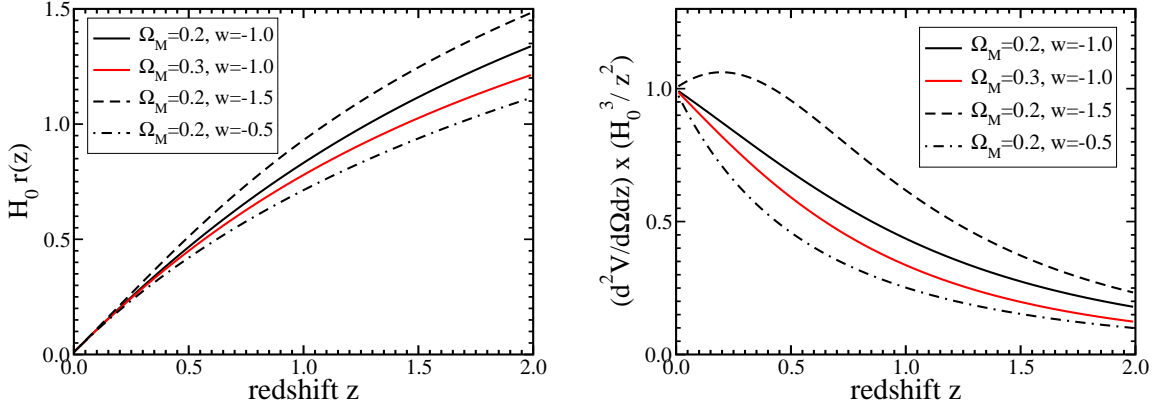


**FIGURE 2.** Left: Distance vs. redshift in a flat Universe with different values of the cosmological parameters  $\Omega_m$  and  $w$ . Right: volume element vs. redshift for same models. From Frieman et al. [13].

where  $\Omega_k = 1 - \Omega_0 = 1 - \Omega_m - \Omega_{DE}$ . For a general dark energy model with equation of state parameter  $w(z)$ , the Hubble expansion rate can be written as

$$\frac{H^2(z)}{H_0^2} = \Omega_m(1+z)^3 + \Omega_{DE} \exp \left[ 3 \int (1+w(z)) d \ln(1+z) \right] + \Omega_k(1+z)^2. \quad (15)$$

For the case of the cosmological constant,  $w = -1$ , this can be rewritten as

$$\frac{H^2(a)}{H_0^2} = \Omega_m a^{-3} + \Omega_\Lambda + \Omega_k a^{-2}, \quad (16)$$

and the luminosity distance becomes

$$d_L(z; \Omega_m, \Omega_\Lambda) = \frac{c(1+z)}{H_0} |\Omega_k|^{-1/2} S_k \left( \int_{1/(1+z)}^1 |\Omega_k|^{1/2} \frac{da}{a^2 [\Omega_m a^{-3} + \Omega_\Lambda + \Omega_k a^{-2}]^{1/2}} \right). \quad (17)$$

Another important special case is a flat Universe ( $\Omega_k = k = 0$ ) and dark energy with  $w =$  constant, independent of redshift. In this case,

$$\frac{H^2(z)}{H_0^2} = (1 - \Omega_{DE})(1+z)^3 + \Omega_{DE}(1+z)^{3(1+w)}, \quad (18)$$

and the luminosity distance is given by

$$d_L(z; \Omega_{DE}, w) = \chi(1+z) = \frac{1+z}{H_0} \int \frac{1 + \Omega_{DE} [(1+z)^{3w} - 1]^{-1/2}}{(1+z)^{3/2}} dz. \quad (19)$$

Note that the product  $H_0 d_L$  is independent of the Hubble parameter  $H_0$ .

The absolute and apparent magnitudes are logarithmic measures of luminosity and flux:  $M_j = -2.5 \log(L_j) + c_1$ ,  $m_i = -2.5 \log(f_i) + c_2$ , where  $i(j)$  denotes the observed(rest-frame) passband. Luminosity distance measurements are then conveniently given in terms of the *distance modulus*,

$$\mu \equiv m_i - M_j = 2.5 \log(L_j/f_i) = 5 \log[H_0 d_L(z; \Omega_m, \Omega_{DE}, w(z))] - 5 \log H_0 + K_{ij}(z), \quad (20)$$

where  $K_{ij}$  is the redshift-dependent K-correction that accounts for the redshifting between the observed and emitted passbands and depends upon the spectral energy distribution of the source. For a population of standard candles (fixed  $M_j$ ) with known spectra ( $K_{ij}$ ), measurements of  $\mu$  vs.  $z$ , the Hubble diagram, constrain cosmological parameters. The parameter dependence of the distance vs. redshift is shown in the left panel of Fig. 2. The right panel shows the comoving volume element,  $d^2V/dz d\Omega = r^2(z)/H(z)$ .

If  $M_j$  is known, then from measurement of  $m_i$  and knowledge of the spectrum we can infer the *absolute* distance to an object at redshift  $z$ ; we can thereby determine  $H_0$ , since  $d_L \simeq cz/H_0$  for  $z \ll 1$ . If  $M_j$  is unknown, then from measurement of  $m_i$  we can infer the distance to an object at redshift  $z_1$  *relative* to an object at redshift  $z_2$ ,  $m_1 - m_2 = 5 \log(d_1/d_2) + K_1 - K_2$ . For supernovae, we typically measure relative distances, using low-redshift supernovae to vertically anchor the Hubble diagram, i.e., to approximately determine the quantity  $M - 5 \log H_0$ .

### SN Discovery

The recognition in the 1990's that supernovae are standardizable candles, together with the availability of large mosaic CCD cameras on 4-meter class telescopes, stimulated two teams, the Supernova Cosmology Project (SCP) and the High- $z$  SN Search Team (HZT), to measure the SN Ia Hubble diagram to much larger distances than was previously possible. Based on samples of tens of objects, both teams found that distant SNe are  $\sim 0.25$  mag dimmer than they would be in a decelerating Universe, indicating that the expansion has been speeding up for the past 5 Gyr [1, 2]; a compilation of the discovery data from the two teams is shown in Fig. 3a. Initially, these results were interpreted in terms of the cosmological constant model, Fig. 3b, using Eqn. 17. The constraint region delineates the values of the parameters  $\Omega_m, \Omega_\Lambda$  which combine to give similar luminosity distance estimates to  $z \sim 0.5$ . The results are also often interpreted in terms of the flat, constant  $w$  model of Eqn. 19, as shown in Fig. 6 below.

## Cosmic Microwave Background Anisotropy

The second important piece of evidence in favor of cosmic acceleration came from the CMB anisotropy. As noted above, the CMB carries the imprint of processes in the photon-baryon fluid around the time of recombination, when the photons last scattered with baryons, at  $z_{ls} = 1089$ . CMB maps, such as those made most recently by the Wilkinson Microwave Anisotropy Probe (WMAP), show the strongest temperature fluctuations

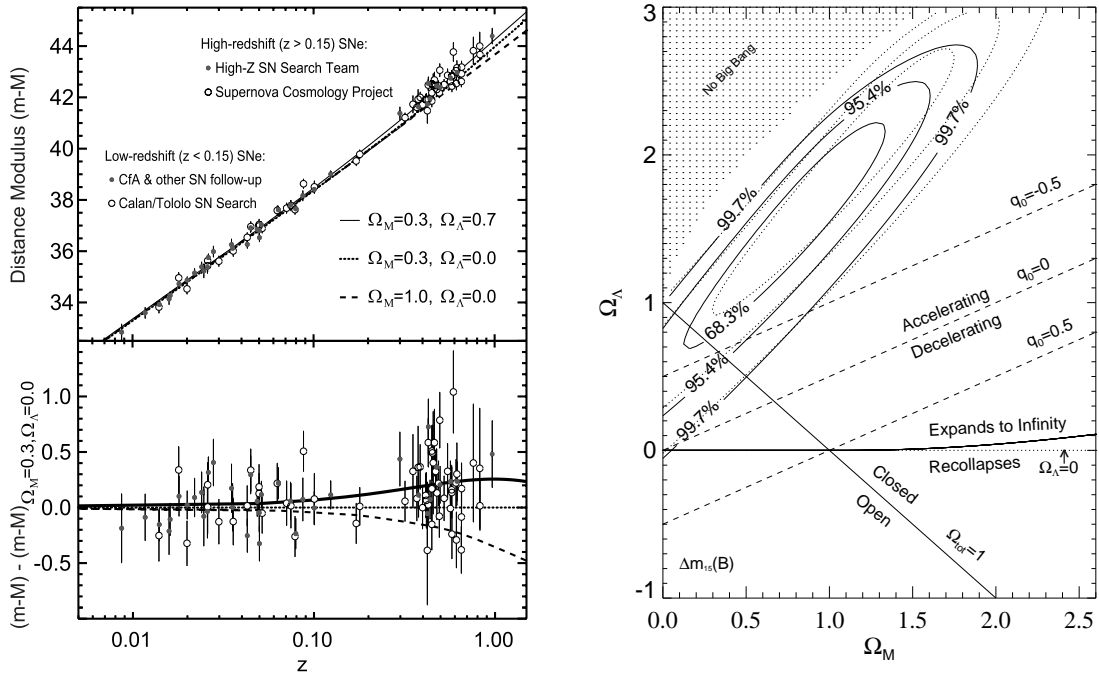


**FIGURE 3.** Left panel (a): Discovery data: Hubble diagram of SNe Ia measured by the SCP and HZT. Bottom panel shows residuals in distance modulus relative to an open universe with  $\Omega_0 = \Omega_m = 0.3$ . Figure adapted from [30, 31], based on [1, 2]. Right panel (b): constraints on  $\Omega_m$  and  $\Omega_\Lambda$  from the HZT data [1].

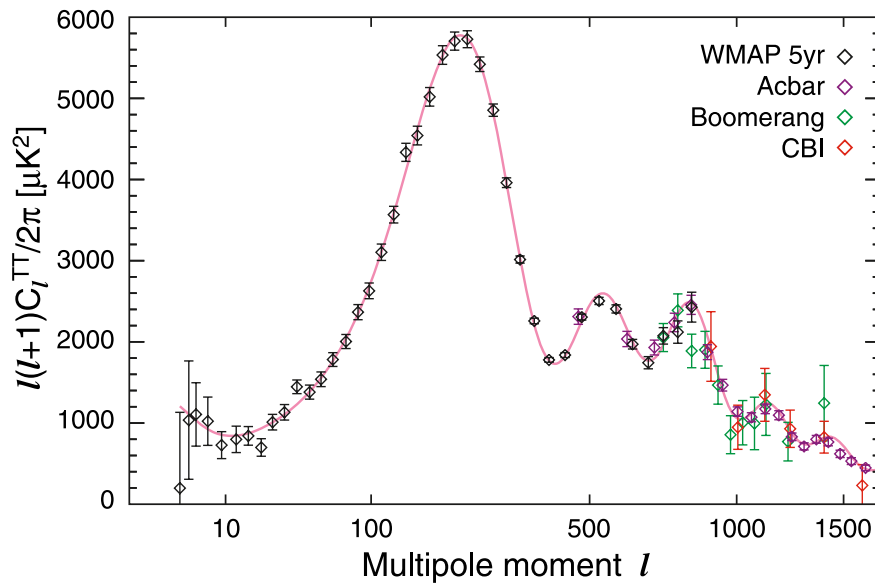


**FIGURE 4.** CMB temperature anisotropy angular power spectrum measurements from WMAP, Acbar, Boomerang, and CBI. From Dunkley et al. [32].

on a characteristic angular scale of about 1 degree. This is the angular scale subtended by the sound horizon,  $s = c_s t_{ls}$ , the distance that gravity-driven sound waves in the photon-baryon fluid can travel before last scattering. More precisely,

$$s = \int_0^{t_{ls}} c_s(1+z)dt = \int_{z_{ls}}^{\infty} \frac{c_s}{H(z)} dz, \quad (21)$$

where the sound speed  $c_s$  is determined by the ratio of the baryon and photon energy densities,  $c_s = [3(1 + 3\rho_b/4\rho_\gamma)]^{-1/2}$ . Before recombination, the sound speed is relativistic, about  $c_s \simeq 0.57c$ , due to the large pressure provided by the CMB photons.

While  $s$  is fixed primarily by  $\Omega_\gamma$  and  $\Omega_b$ , the angular scale subtended by  $s$  is determined primarily by the spatial curvature of the Universe: for  $\Omega_0 > 1$  ( $\Omega_0 < 1$ ), the angular scale is larger (smaller) than it is in a flat Universe. In 2000-2001, the Boomerang, DASI, and MAXIMA experiments [33, 34, 35] reported robust detections of the first acoustic peak in the CMB temperature anisotropy angular power spectrum at an angular scale of about 1 degree, as expected for a nearly flat Universe. In a plot of  $\Omega_\Lambda$  vs.  $\Omega_m$  such as Fig. 3b, the CMB constraints thus lie near the  $\Omega_0 = 1$  line, nearly orthogonal to the supernova constraints; more precisely, the CMB degeneracy line is approximately  $1 - \Omega_0 = -0.3 + 0.4\Omega_\Lambda$ , as shown below in Fig. 6a. Together, the SN and CMB constraints point to a best-fit model with  $\Omega_\Lambda \simeq 0.75$  and  $\Omega_m \simeq 0.25$ . The CMB constraints have been strengthened considerably by recent results from WMAP and from ground-based experiments that probe smaller angular scales. A recent compilation of CMB anisotropy results is shown in Fig. 4, clearly showing the pattern of acoustic oscillations. The WMAP 5-year data constrains the distance to last scattering as [36]

$$R = (\Omega_m H_0^2)^{1/2} \int_0^{z_{ls}} \frac{dz}{H(z)} = 1.715 \pm 0.021. \quad (22)$$

The resulting constraints on cosmological parameters are shown in Fig. 6. The CMB constraints on the dark energy equation of state parameter  $w$  are comparatively weak, due to a large degeneracy between  $w$  and  $\Omega_{DE}$  in determining the angular diameter distance to the last-scattering surface. Nevertheless, the positions and amplitudes of the acoustic peaks in Fig. 4 encode a wealth of cosmological information. CMB measurements are extremely important for present and future dark energy probes since they strongly constrain a variety of cosmological parameters. The upcoming Planck mission is expected to constrain a number of (non-dark energy) cosmological parameters at the  $\sim 1\%$  level.

## Large-scale Structure: Baryon Acoustic Oscillations

The baryon acoustic oscillations (BAO), so prominent in the CMB anisotropy, leave a more subtle imprint in the large-scale distribution of galaxies, a bump in the two-point correlation function  $\xi(r)$  at a scale  $r \sim 110h^{-1}$  Mpc. This is roughly the distance at which an outgoing spherical sound wave in the photon-baryon fluid stalls when the photons and their associated pressure decouple from the baryons at the time of last scattering. The sound waves remain imprinted in the baryon distribution and, through gravita-

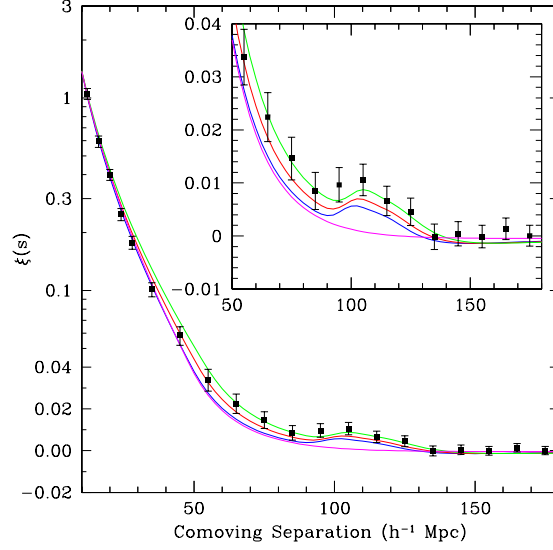


**FIGURE 5.** Correlation function for SDSS luminous red galaxies, showing the expected bump due to BAO on large scales. From Eisenstein et al. [37].

tional interactions, in the dark matter distribution as well. However, since  $\Omega_b/\Omega_m \simeq 1/6$ , dark matter dominates the growth of structure, and the imprint of baryon oscillations in the galaxy distribution is relatively small.

Measurement of the BAO signature in the correlation function of luminous red galaxies in the Sloan Digital Sky Survey (SDSS), shown in Fig. 5, has constrained the distance to the median redshift  $z_1 = 0.35$  of this sample to a precision of 5% [37]. The BAO measurements constrain several different parameters [37, 38], depending on whether and how information from the CMB is used. Eisenstein et al. [37] show that they constrain the combination of angular diameter distance, Hubble parameter, and  $\Omega_m$  given by

$$\begin{aligned}
 A(z_1; w, \Omega_m, \Omega_{DE}) &= \sqrt{\Omega_m} \left( \frac{H_0}{H(z_1)} \right)^{1/3} \left[ \frac{|\Omega_k|^{-1/2}}{z_1} S_k \left( |\Omega_k|^{1/2} \int_0^{z_1} dz \frac{H_0}{H(z)} \right) \right]^{2/3} \\
 &= 0.469 \pm 0.017 .
 \end{aligned} \tag{23}$$

Since this quantity scales with redshift and cosmological parameters in a manner different from the luminosity distance, its measurement carves out a different likelihood region in the space of cosmological parameters. The resulting constraints in the  $w, \Omega_m$  plane are shown in Fig. 6. This figure demonstrates the robustness of the current results: although SN, CMB, and LSS are complementary, one can drop any one of them and still find strong evidence in favor of cosmic acceleration. For evidence from the CMB and LSS alone, see, e.g., [39].

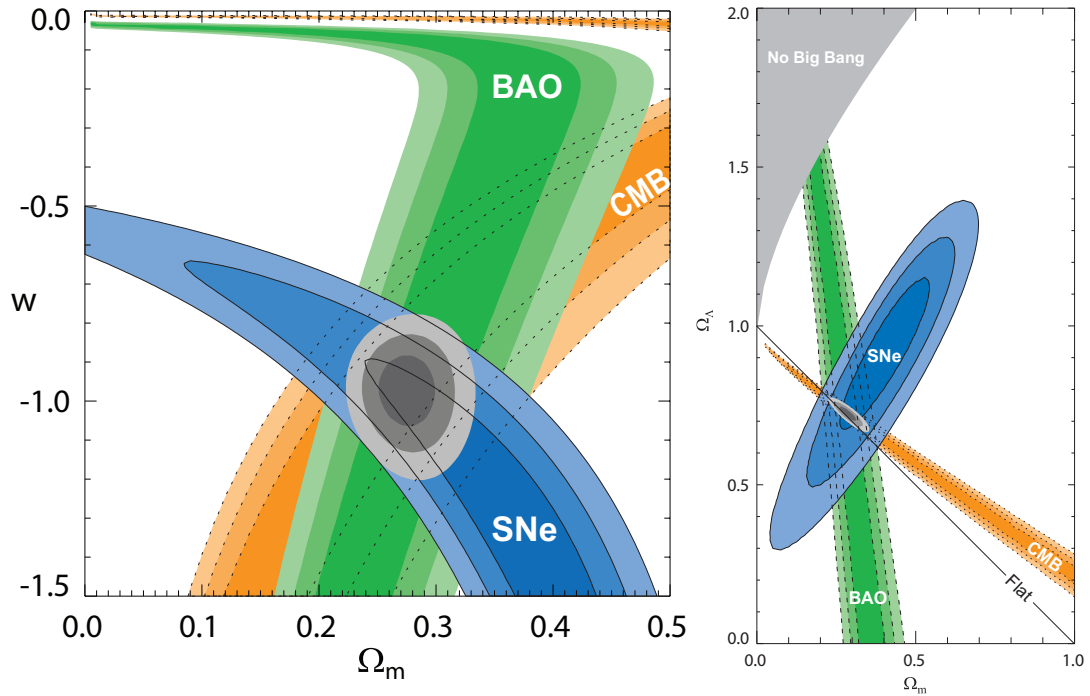


**FIGURE 6.** Left panel (a): recent constraints from SNe, CMB anisotropy (WMAP5), and large-scale galaxy correlations (SDSS BAO) upon the cosmological parameters  $w, \Omega_m$  (for a flat Universe with constant  $w$ ); Right panel (b): constraints upon  $\Omega_m$  and  $\Omega_\Lambda$  for the cosmological constant model ( $w = -1$ ). Statistical errors only are shown. From Kowalski et al. [40].

## CONTINUING EVIDENCE FOR COSMIC ACCELERATION

While CMB and LSS measurements independently strengthened the evidence for an accelerating Universe, subsequent supernova observations have reinforced the original results, and new evidence has accrued from other observational probes. Here we briefly review these recent developments and discuss the current status of our knowledge of dark energy.

### Recent Supernova Observations

A number of concerns were raised about the robustness of the first SN evidence for acceleration, e.g., it was suggested that distant SNe could appear fainter due to extinction by hypothetical grey dust rather than acceleration [41, 42]. Over the intervening decade, the supernova evidence for acceleration has been strengthened by results from a series of SN surveys. Observations with the Hubble Space Telescope (HST) have provided high-quality light curves [43] and have extended SN measurements to redshift  $z \simeq 1.8$ , providing evidence for the expected earlier epoch of deceleration and disfavoring dust extinction as an alternative explanation to acceleration [44, 45, 46].

Two large ground-based surveys, the Supernova Legacy Survey (SNLS) [47] and the

ESSENCE survey [48, 49], have been using 4-meter telescopes to measure light curves for several hundred SNe Ia over the redshift range  $z \sim 0.3 - 0.9$ , with large programs of spectroscopic follow-up on 6- to 10-m telescopes. They have each reported results from a fraction of the total data collected, with more to follow. The quality and quantity of the distant SN data are now vastly superior to what was available in 1998, and the evidence for acceleration is correspondingly more secure. An example of a recent analysis using this larger, more recent combination of supernova data sets is shown in Fig. 6 [40]. In combination with CMB and LSS results (see below), the SN data constrain the equation of state parameter  $w$  to an uncertainty  $\sim 0.08 - 0.15$  for a flat Universe and constant  $w$ , with a central value consistent with the cosmological constant,  $w = -1$ . The range of uncertainty above reflects different assumptions in the literature about the size of systematic errors. On the other hand, if we drop the assumption of non-evolving  $w$ , which is not well motivated if  $w \neq -1$ , then the current constraints are considerably weaker.

## Systematic Errors in SN Distance Estimates

With the substantial advances in the number of supernova distance measurements in recent years and the consequent decline in statistical errors, systematic errors have come into sharper focus as a limiting factor. The major systematic concerns for supernova distance measurements are errors in correcting for host-galaxy extinction and uncertainties in the intrinsic colors of supernovae; luminosity evolution; and selection bias in the low-redshift sample. Even with multi-band observations, the combination of photometric errors, variations in intrinsic SN Ia colors, and uncertainties and likely variations in host-galaxy dust properties lead to significant uncertainties in distance estimates. Observations that extend into the rest-frame near-infrared, such those being carried out by the Carnegie Supernova Project, offer promise in controlling dust-extinction systematics since their effects are much reduced at long wavelengths.

With respect to luminosity evolution, there is evidence that SN peak luminosity correlates with host-galaxy type [e.g., 50], and that the mean host-galaxy environment, e.g., the star formation rate, evolves strongly with look-back time. However, brightness-decline-corrected SN Ia Hubble diagrams are consistent between different galaxy types, and since the nearby Universe spans the range of galactic environments sampled by the high-redshift SNe, one can measure distances to high-redshift events by comparing with low-redshift analogs. While SNe provide a number of correlated observables (multi-band light curves and multi-epoch spectra) to constrain the physical state of the system, insights from SN Ia theory will likely be needed to determine if they are collectively sufficient to constrain the mean peak luminosity at the percent level required for future dark energy missions [27].

Finally, there is concern that the low-redshift SNe currently used to anchor the Hubble diagram and that serve as templates for fitting distant SN light curves are a relatively small, heterogeneously selected sample and that correlated large-scale peculiar velocities induce larger distance errors than previously estimated [51]. This situation should improve in the near future once results are collected from low-redshift SN surveys such

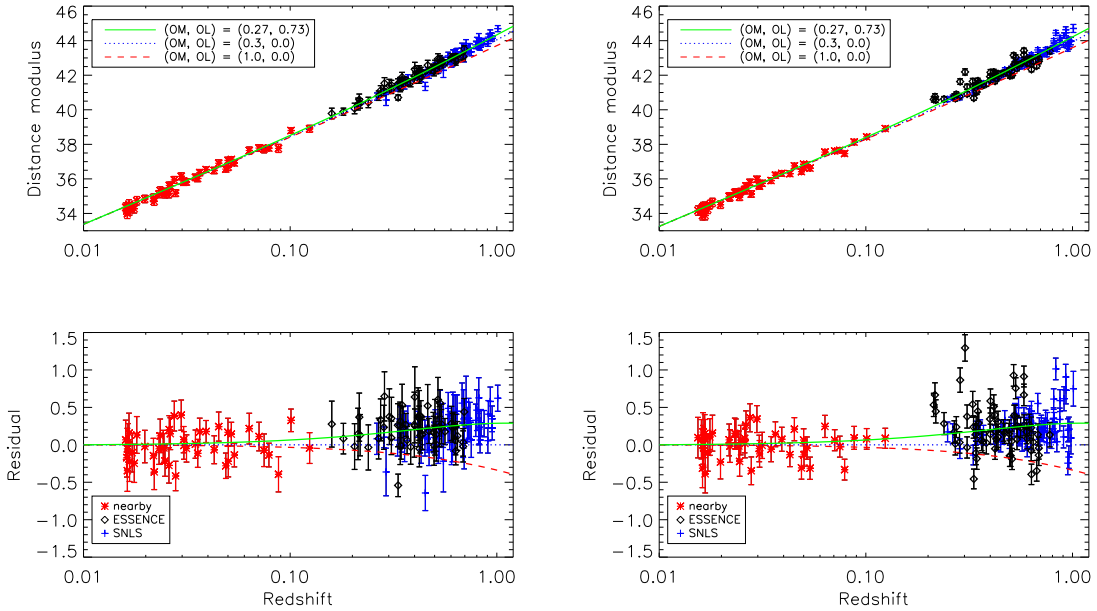


**FIGURE 7.** Hubble diagram for low-redshift (red), SNLS (blue), and ESSENCE (black) supernovae using the MLCS2k2 distance estimator (left panel) and the SALT2 fitter (right panel). Lower panels show residuals from an open model with  $\Omega_m = 0.3, \Omega_\Lambda = 0$ . From Wood-Vasey et al. [49].

as the Lick Observatory Supernova Search (LOSS), the Center for Astrophysics Supernova project, the Carnegie Supernova Project, the Nearby Supernova Factory, and the SDSS-II Supernova Survey. Over the course of three 3-month seasons, the latter survey discovered and measured multi-band light curves for nearly 500 spectroscopically confirmed SNe Ia in the redshift range  $z \sim 0.05 - 0.4$ , filling in the “redshift desert” between low- and high-redshift samples that is evident in Fig. 7 [52, 53].

One illustration of systematic error concerns is provided by Fig. 7, which shows the Hubble diagram for the same published low-redshift, ESSENCE, and SNLS data analyzed using two different light-curve fitters, the multi-color light-curve shape (MLCS) method [50] and SALT [54, 55]. One sees significant differences in distance estimates, and the best-fit values of  $w$ , using the SNe plus BAO constraints, differ by about 0.11. These fitters take different approaches to SN distance estimation. MLCS is based on *UVBRI* rest-frame light-curve templates derived from well-observed nearby supernovae. It incorporates a brightness vs. light-curve shape correlation and assumes that color variations not associated with the brightness-shape relation are due to dust extinction in the host galaxy. Host-galaxy dust is modeled using a derived extinction vs. wavelength relation for the Milky Way, and a prior on the amplitude of the dust extinction is imposed, again based on observations of the low-redshift supernovae. SALT, by contrast, begins with rest-frame spectral templates that are synthesized to produce broad-band model photometry. It incorporates a brightness-shape correlation and an empirical color variation that is not required to emulate the effects of dust but that appears to match the wavelength dependence of dust extinction reasonably well. In particular, there are no



explicit assumptions about dust and no associated priors. However, the translation of light-curve shape and color variations into luminosity and therefore distance variations is controlled by two global parameters that are determined in a simultaneous fit of model and cosmological parameters to the Hubble diagram. As a result, SALT does not yield cosmology-independent distance estimates for each supernova, and SALT SN distances derived in the context of a particular cosmology parametrization (e.g.,  $k = 0$  and constant  $w$ ) should not be applied to constrain other models.

Accounting for systematic errors, precision measurement of  $w$  and particularly of its evolution with redshift will require a few thousand SN Ia light curves out to redshifts  $z \sim 1.5$  to be measured with unprecedented precision and control of systematics [56]. For redshifts  $z > 0.8$ , this will require going to space to minimize photometric errors, to obtain uniform light-curve coverage, and to observe in the near-infrared bands to capture the redshifted photons.

## Corroborating Evidence for Acceleration

A number of observations made in the last several years have provided additional evidence for cosmic acceleration. We highlight some of the major developments here.

**Integrated Sachs-Wolfe effect:** The presence of dark energy affects the large-angle anisotropy of the CMB (the low- $\ell$  multipoles). This Integrated Sachs-Wolfe (ISW) effect arises due to the differential redshifts of photons as they pass through time-changing gravitational potential wells, and it leads to a small correlation between the low-redshift matter distribution and the CMB temperature anisotropy. This effect has been observed in the cross-correlation of the CMB with galaxy and radio source catalogs [57, 58, 59, 60]. This signal indicates that the Universe is not described by the Einstein-de Sitter model ( $\Omega_m = 1$ ), a reassuring cross-check.

**Weak gravitational lensing** [61, 62], the small, correlated distortions of galaxy shapes due to gravitational lensing by intervening large-scale structure, is a powerful technique for mapping dark matter and its clustering. Detection of this cosmic shear signal was first announced by four groups in 2000 [63, 64, 65, 66]. Recent lensing surveys covering areas of order 100 square degrees have shed light on dark energy by pinning down the combination  $\sigma_8(\Omega_m/0.25)^{0.6} \approx 0.85 \pm 0.07$ , where  $\sigma_8$  is the rms amplitude of mass fluctuations on the  $8 h^{-1}$  Mpc scale [67, 68, 69]. Since other measurements peg  $\sigma_8$  at  $\simeq 0.8$ , this implies that  $\Omega_m \simeq 0.25$ , consistent with a flat Universe dominated by dark energy. In the future, weak lensing has the potential to be a very powerful probe of dark energy [70, 71], as discussed below.

**X-ray Clusters:** Measurements of the ratio of X-ray emitting gas to total mass in galaxy clusters,  $f_{\text{gas}}$ , also indicate the presence of dark energy. Since galaxy clusters are the largest collapsed objects in the universe, the gas fraction in them is presumed to be constant and nearly equal to the baryon fraction in the Universe,  $f_{\text{gas}} \approx \Omega_b/\Omega_m$  (most of the baryons in clusters reside in the gas). The value of  $f_{\text{gas}}$  inferred from observations depends on the observed X-ray flux and temperature as well as the distance to the cluster. Only the “correct cosmology” will produce distances which make the apparent  $f_{\text{gas}}$  constant in redshift. Using data from the Chandra X-ray Observatory, Allen et al.

[72], Allen et al. [73] determined  $\Omega_\Lambda$  to a 68% precision of about  $\pm 0.2$ , obtaining a value consistent with the SN data.

**Strong Lensing:** A distant quasar lying near the line of sight to a foreground galaxy can have its light strongly bent by the galaxy's gravitational field. In favorable circumstances, this leads to the appearance of multiple images of the same quasar, an instance of strong gravitational lensing. Schematically, the optical depth for lensing can be written

$$\tau(z_S) = \int dV \int dM \frac{dn}{dM} A_L(M), \quad (24)$$

where  $dV$  is the volume element, the volume integral is taken out to the QSO redshift  $z_S$ ,  $dn/dM$  is the redshift-dependent mass function of the lens population (assumed to be massive galaxies and their associated dark matter halos), and  $A_L(M)$  is determined by the density profiles of the lenses, often modeled as singular isothermal spheres for galaxy-scale lenses. In principle, the volume element is strongly sensitive to the cosmological constant (see Fig. 2), so the optical depth for strong lensing would seem a natural dark energy probe [74, 75]. However, a major difficulty arises from the fact that the mass function of the lens population is not an observable. Traditionally, galaxy scaling relations such as the Faber-Jackson relation between luminosity and velocity dispersion, along with measurements of the galaxy luminosity function  $dn/dL$ , were used to infer the galaxy mass function  $dn/dM$ , but the associated uncertainties, particularly for galaxies at  $z \sim 0.5$  that dominate the optical depth, were large. More recent approaches have made use of the velocity-dispersion distribution function of early-type galaxies,  $dn/d\sigma_v$ , measured, e.g., by the SDSS [76, 77, 78]. Fig. 8 shows examples of recent constraints on  $\Omega_\Lambda$  and  $\Omega_m$  (for  $w = -1$ ) and on  $\Omega_m$  and  $w$  (for a flat Universe) from strong lens statistics. While the statistical errors are large, the results are consistent with an accelerating Universe.

## MODELS OF COSMIC ACCELERATION

Understanding the origin of cosmic acceleration presents both a challenge and an opportunity to theorists. While there has been no shortage of ideas, there is also no consensus model. In this section, we briefly review the theoretical landscape.

### Dark Energy Models

#### *Vacuum Energy*

Vacuum energy is the simplest candidate for dark energy. As noted above, since the stress-energy of the vacuum  $T_{\mu\nu}^{vac}$  is proportional to the metric  $g_{\mu\nu}$ , it is mathematically equivalent to a cosmological constant. The difficulty arises when one attempts to calculate its expected value. For each mode of a quantum field there is a zero-point energy

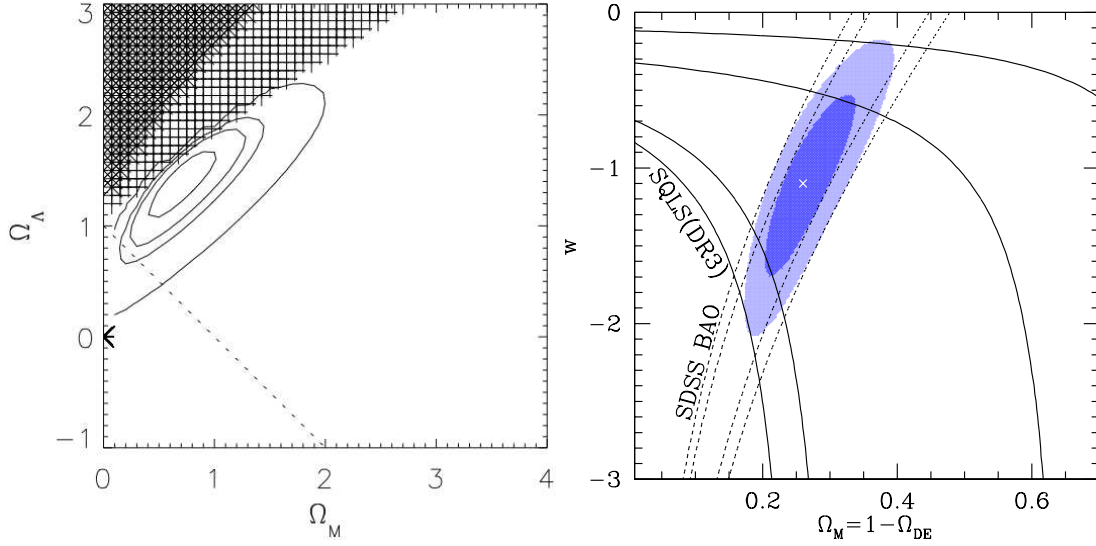


**FIGURE 8.** Constraints on dark energy from the statistics of strongly lensed QSOs. Left panel: constraints on  $\Omega_\Lambda, \Omega_m$  from the CLASS lens survey, from Mitchell et al. [76]. Right panel: constraints on  $w, \Omega_m$  from the SDSS lensed QSO survey (black), from SDSS BAO (dotted), and the combination of the two (blue), from Oguri et al. [77].

$\hbar\omega/2$ , so that the energy density of the quantum vacuum is given by

$$\rho_{vac} = \frac{1}{2} \sum_{\text{fields}} g_i \int_0^\infty \sqrt{k^2 + m^2} \frac{d^3k}{(2\pi)^3} \simeq \sum_{\text{fields}} \frac{g_i k_{\text{max}}^4}{16\pi^2}, \quad (25)$$

where  $g_i$  accounts for the degrees of freedom of the field (the sign of  $g_i$  is + for bosons and – for fermions), and the sum runs over all quantum fields (quarks, leptons, gauge fields, etc). Here  $k_{\text{max}}$  is an imposed momentum cutoff, because the sum diverges quartically.

To illustrate the magnitude of the problem, if the energy density contributed by just one field is to be at most the critical density, then the cutoff  $k_{\text{max}}$  must be  $< 0.01$  eV — well below the energy scale where one could have appealed to ignorance of physics beyond. Taking the cutoff to be the Planck scale ( $\approx 10^{19}$  GeV), where one expects quantum field theory in a classical spacetime metric to break down, the zero-point energy density would exceed the critical density by 120 orders of magnitude. It is highly unlikely that a classical contribution to the vacuum energy density would cancel this quantum contribution to such high precision. This large discrepancy is known as the cosmological constant problem [12].

Supersymmetry, the hypothetical symmetry between bosons and fermions, appears to provide only partial help. In a supersymmetric (SUSY) world, every fermion in the standard model of particle physics has an equal-mass SUSY bosonic partner and vice versa, so that fermionic and bosonic zero-point contributions to  $\rho_{vac}$  would exactly cancel. However, SUSY is not a manifest symmetry in Nature: none of the SUSY particles has yet been observed in collider experiments, so they must be substantially heavier than their standard-model partners. If SUSY is spontaneously broken at a mass

scale  $M$ , one expects the imperfect cancellations to generate a finite vacuum energy density  $\rho_{vac} \sim M^4$ . For the currently favored value  $M \sim 1$  TeV, this leads to a discrepancy of 60 (as opposed to 120) orders of magnitude with observations.

One approach to the cosmological constant problem involves the idea that the vacuum energy scale is a random variable that can take on different values in different disconnected regions of the Universe. Because a value much larger than that needed to explain the observed cosmic acceleration,  $\rho_{vac} > 125\rho_{crit}$ , would preclude the formation of galaxies (assuming all other cosmological parameters are held fixed), we could not find ourselves in a region with such large  $\rho_{vac}$  [79]. Imagining an ensemble of universes or of such disconnected large regions, the probability for us to observe a particular value of  $\rho_{vac}$  is given by [79]  $dP(\rho_{vac}) = P^*(\rho_{vac})N(\rho_{vac})d\rho_{vac}$ , where  $P^*(\rho_{vac})$  is the prior probability for a region to have a given value of the vacuum energy density. Here,  $N(\rho_{vac})$  is the fraction of baryons that end up in galaxies or in systems large enough to sustain observers and has support only at  $\rho_{vac} < 125\rho_{crit}$  (again holding all other parameters fixed, including the amplitude of primordial perturbations). Weinberg [79] assumed that  $P^*$  is broad and effectively constant over the anthropically allowed range of  $N$ . Vilenkin and Rubakov, however, have noted that  $P^*$  could vary strongly over this range and could in fact be strongly peaked at large values of  $\rho_{vac}$ . In that case, we would be more likely to find ourselves living “on the edge” of the allowed region, and life should be nasty, brutish, and short, a view one might term the misanthropic principle.

The anthropic approach finds a possible home in the landscape version of string theory, in which the number of different vacuum states is very large and essentially all values of the cosmological constant are possible. Provided that the Universe has such a multiverse structure, this might provide an explanation for the smallness of the cosmological constant [80, 81].

### *Light Scalar Fields*

Another approach to dark energy involves the idea that the Universe is not yet in its ground state. Suppose the true vacuum energy is zero (for reasons yet unknown),  $\Lambda = 0$ . Transient vacuum-like energy can exist if there is a field that takes a cosmologically long time to reach its ground state [82, 83, 22, 84]. This was the reasoning behind primordial inflation, a proposed epoch of accelerated expansion in the very early universe. For this reasoning to apply now, we must postulate the existence of an extremely light scalar field  $\phi$ , since the dynamical timescale for evolution of such a field is given by  $t_\phi \sim 1/m_\phi$ . To satisfy  $t_\phi > 1/H_0$ , the scalar mass should satisfy  $m_\phi < H_0 \sim 10^{-33}$  eV, extremely tiny by particle physics standards for fields that are not exactly massless due to a symmetry. Since the Compton wavelength of the field is also of order  $1/H_0 = 3000h^{-1}$  Mpc or larger, it will not gravitationally cluster with large-scale structure—we expect it to be nearly smoothly distributed—though it can have small-amplitude perturbations on the largest observable scales today, which can affect the CMB anisotropy, e.g., [85].

For a scalar field  $\phi$ , with Lagrangian density  $\mathcal{L} = \frac{1}{2}\partial^\mu\phi\partial_\mu\phi - V(\phi)$ , the stress-energy takes the form of a perfect fluid, with

$$\rho = \dot{\phi}^2/2 + V(\phi) \quad , \quad p = \dot{\phi}^2/2 - V(\phi) \quad , \quad (26)$$

where  $\phi$  is assumed to be spatially homogeneous, i.e.,  $\phi(\vec{x}, t) = \phi(t)$ ,  $\dot{\phi}^2/2$  is the kinetic energy, and  $V(\phi)$  is the potential energy. The evolution of the field is governed by its equation of motion,

$$\ddot{\phi} + 3H\dot{\phi} + V'(\phi) = 0, \quad (27)$$

where a prime denotes differentiation with respect to  $\phi$ . Scalar-field dark energy can be described by the equation-of-state parameter

$$w_\phi = \frac{\dot{\phi}^2/2 - V(\phi)}{\dot{\phi}^2/2 + V(\phi)} = \frac{-1 + \dot{\phi}^2/2V}{1 + \dot{\phi}^2/2V}. \quad (28)$$

If the scalar field evolves slowly,  $\dot{\phi}^2/2V \ll 1$ , as it generally will do when  $m_\phi = \sqrt{V''(\phi)} \ll H(t)$ , then  $w_\phi \approx -1$ , and the scalar field behaves like a slowly varying vacuum energy, with  $\rho_{vac}(t) \simeq V[\phi(t)]$ . If this inequality is only marginally satisfied, however, then the equation of state parameter can deviate significantly from  $-1$ , and it generally evolves in time.

The simplest such model would involve just a free, massive scalar field  $V(\phi) = m_\phi^2 \phi^2/2$ . In this case, in order for the field to both supply negative pressure (and therefore drive accelerated expansion) and have the correct magnitude of the energy density,  $\rho \sim 10^{-10} \text{ eV}^4$ , the field amplitude must be very large,  $\phi \sim 10^{28} \text{ eV} \sim M_{Pl}$ , comparable to the Planck mass. This implies that the scalar potential is remarkably flat; one measure of this is that  $m_\phi/\phi \sim 10^{-61}$  or smaller. Moreover, in order not to destroy the required flatness of the potential, the quartic self-coupling of the field,  $\lambda \phi^4/4$ , is constrained to be extremely small,  $\lambda < 10^{-122}$ . These are generic features of scalar field dark energy models. Understanding such very small numbers and ratios makes it challenging to connect scalar field dark energy with particle physics models. In constructing theories that go beyond the standard model of particle physics, including those that incorporate primordial inflation, model-builders have been strongly guided by the requirement that any small dimensionless numbers in the theory should be protected by symmetries from large quantum corrections; such small numbers are then said to be ‘‘technically natural’’. Thus far, this kind of model-building discipline has not been the rule among cosmologists working on dark energy models.

One scenario that does attempt to incorporate the naturalness criterion has a pseudo-Nambu-Goldstone boson as the dark energy scalar [22]. In the simplest incarnation, a global  $U(1)$  symmetry is spontaneously broken at a very high energy scale,  $f \sim M_{Pl}$ , giving rise to a massless Nambu-Goldstone boson. If the symmetry is explicitly broken at a much lower scale  $M \sim 10^{-3} \text{ eV}$  (which is technically natural), then the field gets a tiny mass from the explicit breaking, with a periodic potential of the form

$$V(\phi) = M^4 \left[ 1 + \cos\left(\frac{\phi}{f}\right) \right]. \quad (29)$$

Such a field would be a much lighter cousin of the QCD axion. Examples of particle physics model-building incorporating this idea are given in [86, 87].

In the examples above, at early times the field is frozen to its initial value by the friction term  $3H\dot{\phi}$  in Eqn. 27, and it acts as vacuum energy; when the expansion rate drops below  $H^2 = V''(\phi)$ , the field begins to roll and  $w$  evolves away from  $-1$ . In other

models, the field instead may roll more slowly as time progresses, i.e., the slope of the potential drops more rapidly than the Hubble friction term. This can happen if, e.g.,  $V(\phi)$  falls off exponentially or as an inverse power-law at large  $\phi$ . These “thawing” and “freezing” models tend to carve out different trajectories of  $w(z)$ , so that precise cosmological measurements might be able to discriminate between them [88].

As Fig. 1 shows, through most of the history of the Universe, dark matter or radiation dominated dark energy by many orders of magnitude. We happen to live around the time that dark energy has become important. Is this coincidence between  $\rho_{DE}$  and  $\rho_m$  an important clue to understanding cosmic acceleration or just a natural consequence of the different scalings of cosmic energy densities and the longevity of the Universe? In some freezing models, the scalar field energy density tracks that of the dominant component (radiation or matter) at early times and then dominates at late times, providing a dynamical origin for the coincidence. In thawing models, the coincidence is indeed transitory and just reflects the mass scale of the scalar field.

## Modified Gravity

An alternative approach seeks to explain cosmic acceleration not in terms of dark energy but as a manifestation of new gravitational physics. Instead of adding a new component  $T_{\mu\nu}^{DE}$  to the right side of the Einstein equations (Eqn. 10), one instead modifies the geometric side—schematically,  $G_{\mu\nu} \rightarrow G_{\mu\nu} + f(g_{\mu\nu})$ . A number of ideas have been explored along these lines, from models motivated by higher-dimensional theories and string theory [89, 90] to phenomenological modifications of the Einstein-Hilbert action of General Relativity [91, 92].

As an example, consider the model of Dvali et al. [89], which arises by assuming that we live in a 3-dimensional brane in a 4 + 1-dimensional Universe. The action can be written as

$$S = M_5^3 \int d^5 X \sqrt{|\det g_5|} R_5 + M_{Pl}^2 \int d^4 x \sqrt{|\det g_4|} R_4 + \int d^4 x \sqrt{|\det g_4|} L_m , \quad (30)$$

where the first term is the 5-dimensional Einstein-Hilbert action, the second describes the curvature of the brane, and the third describes the particles of the Standard Model, confined to the brane. At large distances, gravity can leak off the 3-brane into the bulk, infinite 5th dimension. The cross-over from effective 4D to 5D gravity occurs at a scale  $r_c = M_{Pl}^2/M_5^3$  and gives rise to a modified Friedmann equation,

$$H^2 \pm \frac{H}{r_c} = \frac{8\pi G\rho}{3} . \quad (31)$$

Choosing the minus sign in the second term, which becomes important when  $H \sim r_c^{-1}$ , one finds an asymptotically self-accelerating solution,  $H \rightarrow H_\infty = r_c^{-1}$ , even though there is no cosmological constant or vacuum energy term in the action. For acceleration to set in at recent epochs requires the five-dimensional gravitational scale to be of order  $M_5 \sim 1$  GeV. While attractive, it is not clear that a consistent model with this dynamical behavior exists [93].

In the phenomenological approach, one modifies the Einstein-Hilbert action,

$$S = \int d^4x \sqrt{|\det g|} R \rightarrow \int d^4x \sqrt{|\det g|} [M_{Pl}^2 R + f(R, R_{\mu\nu}, R_{\mu\nu\alpha\beta})] , \quad (32)$$

and looks for suitable choices of  $f(R, \dots)$  that induce late acceleration [91, 92]. A challenge for this approach is that the physical effects which typically give rise to corrections to the gravitational action, e.g., the effects of quantum fields in curved spacetime, generally involve positive quadratic forms, e.g.,  $f(R) \sim R^2 + \dots$ . In that case, by dimensional analysis, the correction is only important at very high values of the curvature,  $R \sim M_{Pl}^2$ . To obtain effects at very low curvature, i.e., late cosmic epochs, requires inverse powers of the curvature invariants entering in  $f$ . Solar system tests of General Relativity place stringent constraints on such models.

An interesting feature of modified gravity theories is that they typically imply a modification of the General Relativity relationship between the growth rate of large-scale density perturbations,  $\delta \equiv \delta\rho_m(\mathbf{x}, t)/\bar{\rho}_m$ , and the cosmic expansion rate  $H(t)$ . In General Relativity, the growth of small-amplitude, matter-density perturbations on scales smaller than the Hubble radius is governed by

$$\ddot{\delta} + 2H\dot{\delta} - 4\pi G\bar{\rho}_m\delta = 0 . \quad (33)$$

In the context of General Relativity, dark energy affects the growth of structure through its impact on the expansion rate  $H$ . If acceleration instead arises from a modification of General Relativity, those modifications lead to additional terms in Eqn. 33 that can directly affect the growth rate of large-scale structure. As a result, comparing probes of the expansion rate, e.g., through cosmic distance measurements, with probes of the growth rate of large-scale structure can in principle test the consistency of General Relativity (plus dark energy) as the explanation for acceleration.

## Anthropocentric Universe

Instead of modifying the right or left side of the Einstein equations to explain the supernova observations, a third logical possibility is to drop the assumption that the Universe is spatially homogeneous on large scales. It has been argued that the non-linear gravitational effects of spatial density perturbations, when averaged over large scales, could yield a distance-redshift relation in our observable patch of the Universe that is very similar to that for an accelerating, homogeneous Universe [94], obviating the need for either dark energy or modified gravity. While there has been debate about the amplitude of these effects, this idea has helped spark renewed interest in a class of exact, inhomogeneous cosmologies. For such Lemaître-Tolman-Bondi models to be consistent with the SN data and not conflict with the isotropy of the CMB, the Milky Way must be near the center of a very large-scale, nearly spherical, underdense region [95, 96, 97]. Requiring our galaxy to occupy a privileged location, in violation of the spirit of the Copernican principle, is not yet theoretically well-motivated. However, it remains an interesting empirical question whether such models can be made consistent with the wealth of precision cosmological data [98].

## PROBING DARK ENERGY AND COSMIC ACCELERATION

Although the phenomenon of accelerated expansion is now well established, the underlying physical cause remains a mystery. Is it dark energy or modified gravity? The primary question we would like to address in the near term is whether the cosmological constant (or vacuum energy) can be excluded as the explanation of acceleration: is General Relativity plus dark energy with  $w = -1$  viable or not? Such a model is consistent with all the extant data, so the possibility of excluding it will require much more precise measurements of both the history of the cosmic expansion rate and the history of the growth of large-scale structure. To illustrate the challenge, consider that for fixed  $\Omega_{DE}$ , a 1% change in (constant)  $w$  translates to only a 3% (0.3%) change in dark-energy (total) density at redshift  $z = 2$  and only a 0.2% change in distances to redshifts  $z = 1 - 2$ .

Four methods hold particular promise in probing cosmic acceleration: type Ia supernovae, baryon acoustic oscillations, clusters of galaxies, and weak gravitational lensing. We have described SNe and BAO above; they both provide geometric probes of the expansion rate. Clusters and weak lensing, which we discuss below, are sensitive to both the expansion rate and the growth of structure. As a result, these four probes are complementary in terms of both dark energy constraints as well as the systematic errors to which they are susceptible. Because of this, a multi-pronged approach will be most effective. The goals of the next generation of dark energy experiments will be to constrain the dark energy equation of state parameter  $w$  at the few percent level in order to address the questions above.

### Clusters

Galaxy clusters are the largest virialized objects in the Universe. Within the context of the cold dark matter paradigm for the formation of large-scale structure, the number density of cluster-sized dark matter halos as a function of redshift and halo mass can be accurately predicted from N-body simulations [99, 100]. Comparing these predictions to large-area cluster surveys that extend to high redshift ( $z \sim 1$ ) can provide precise constraints on the cosmic expansion history [101, 102].

The redshift distribution of clusters in a survey that selects clusters according to some observable  $O$  with redshift-dependent selection function  $f(O, z)$  is given by

$$\frac{d^2N(z)}{dzd\Omega} = \frac{r^2(z)}{H(z)} \int_0^\infty f(O, z) dO \int_0^\infty p(O|M, z) \frac{dn(z)}{dM} dM, \quad (34)$$

where  $dn(z)/dM$  is the space density of dark halos in comoving coordinates, and  $p(O|M, z)$  is the mass-observable relation, the probability that a halo of mass  $M$  at redshift  $z$  is observed as a cluster with observable property  $O$ . The utility of this probe hinges on the ability to robustly associate cluster observables such as X-ray luminosity or temperature, cluster galaxy richness, Sunyaev-Zel'dovich effect flux decrement, or weak lensing shear, with cluster mass [e.g., 103].

The sensitivity of cluster counts to dark energy arises from two factors: *geometry*, the term multiplying the integral in Eqn. (34) is the comoving volume element; and *growth*



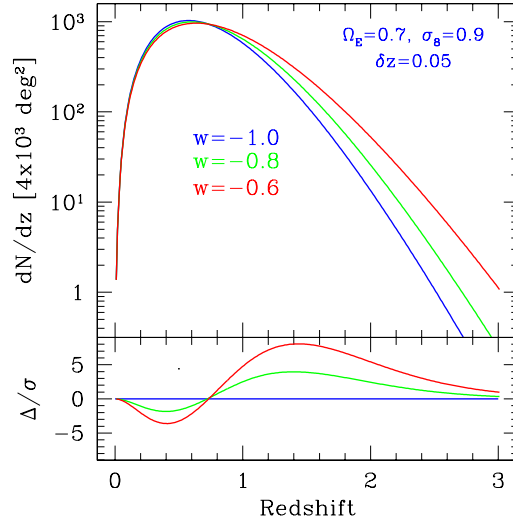


**FIGURE 9.** Predicted cluster counts for a survey covering 4,000 sq. deg. that is sensitive to halos more massive than  $2 \times 10^{14} M_\odot$ , for 3 flat cosmological models with fixed  $\Omega_m = 0.3$  and  $\sigma_8 = 0.9$ . Lower panel shows differences between the models relative to the statistical errors. From Mohr [104].

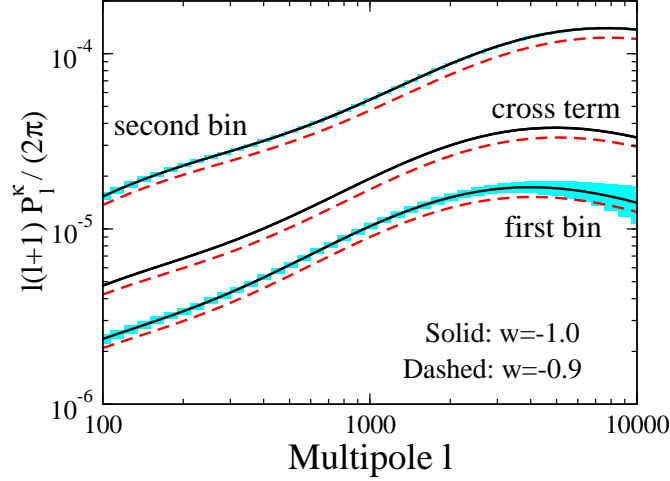
of structure,  $dn(z)/dM$  depends on the evolution of density perturbations, cf. Eqn. 33. The cluster mass function is also determined by the primordial spectrum of density perturbations; its near-exponential dependence upon mass is the root of the power of clusters to probe dark energy.

Fig. 9 shows the sensitivity to the dark energy equation of state parameter of the expected cluster counts for the South Pole Telescope and the Dark Energy Survey. At modest redshift,  $z < 0.6$ , the differences are dominated by the volume element; at higher redshift, the counts are most sensitive to the growth rate of perturbations.

The primary systematic concerns for the cluster method are uncertainties in the mass-observable relation  $p(O|M, z)$  and in the selection function  $f(O, z)$ . The strongest cosmological constraints arise for those cluster observables that are most strongly correlated with mass, i.e., for which  $p(O|M, z)$  is narrow for fixed  $M$ , and which have a well-determined selection function. There are several independent techniques both for detecting clusters and for estimating their masses using observable proxies. Future surveys will aim to combine two or more of these techniques to cross-check cluster mass estimates and thereby control systematic error. Measurement of the spatial correlations of clusters and of the shape of the mass function provide additional internal calibration of the mass-observable relation [105, 106].

## Weak Lensing

The gravitational bending of light by structures in the Universe distorts or shears the images of distant galaxies. This distortion allows the distribution of dark matter and



**FIGURE 10.** Cosmic shear angular power spectrum and statistical errors expected for LSST for  $w = -1$  and  $-0.9$ . For illustration, results are shown for source galaxies in two broad redshift bins,  $z_s = 0 - 1$  (first bin) and  $z_s = 1 - 3$  (second bin); the cross-power spectrum between the two bins (cross term) is shown without the statistical errors. From Frieman et al. [13].

its evolution with time to be measured, thereby probing the influence of dark energy on the growth of structure. The statistical signal due to gravitational lensing by large-scale structure is termed “cosmic shear.” The cosmic shear field at a point in the sky is estimated by locally averaging the shapes of large numbers of distant galaxies. The primary statistical measure of the cosmic shear is the shear angular power spectrum measured as a function of source-galaxy redshift  $z_s$ . (Additional information is obtained by measuring the correlations between shears at different redshifts or with foreground lensing galaxies.) The shear angular power spectrum is [107, 108]

$$P_\ell^\gamma(z_s) = \int_0^{z_s} dz \frac{H(z)}{d_A^2(z)} |W(z, z_s)|^2 P_\rho \left( k = \frac{\ell}{d_A(z)}; z \right), \quad (35)$$

where  $\ell$  denotes the angular multipole, the weight function  $W(z, z_s)$  is the efficiency for lensing a population of source galaxies and is determined by the distance distributions of the source and lens galaxies, and  $P_\rho(k, z)$  is the power spectrum of density perturbations.

As with clusters, the dark-energy sensitivity of the shear angular power spectrum comes from two factors: *geometry*—the Hubble parameter, the angular-diameter distance, and the weight functions; and *growth of structure*—through the evolution of the power spectrum of density perturbations. It is also possible to separate these effects and extract a purely geometric probe of dark energy from the redshift dependence of galaxy-shear correlations [109, 110]. The three-point correlation of cosmic shear is also sensitive to dark energy [111].

The statistical uncertainty in measuring the shear power spectrum on large scales is [107]

$$\Delta P_\ell^\gamma = \sqrt{\frac{2}{(2\ell+1)f_{\text{sky}}}} \left[ P_\ell^\gamma + \frac{\sigma^2(\gamma_i)}{n_{\text{eff}}} \right], \quad (36)$$

where  $f_{\text{sky}}$  is the fraction of sky area covered by the survey,  $\sigma^2(\gamma_i)$  is the variance in a single component of the (two-component) shear, and  $n_{\text{eff}}$  is the effective number density per steradian of galaxies with well-measured shapes. The first term in brackets, which dominates on large scales, comes from cosmic variance of the mass distribution, and the second, shot-noise term results from both the variance in galaxy ellipticities (“shape noise”) and from shape-measurement errors due to noise in the images. Fig. 10 shows the dependence on the dark energy of the shear power spectrum and an indication of the statistical errors expected for a survey such as that planned for LSST, assuming a survey area of 15,000 sq. deg. and effective source galaxy density of  $n_{\text{eff}} = 30$  galaxies per sq. arcmin.

Systematic errors in weak lensing measurements arise from a number of sources [112]: incorrect shear estimates, uncertainties in galaxy photometric redshift estimates, intrinsic correlations of galaxy shapes, and theoretical uncertainties in the mass power spectrum on small scales. The dominant cause of galaxy shape measurement error in current lensing surveys is the anisotropy of the image point spread function (PSF) caused by optical and CCD distortions, tracking errors, wind shake, atmospheric refraction, etc. This error can be diagnosed since there are geometric constraints on the shear patterns that can be produced by lensing that are not respected by systematic effects. A second kind of shear measurement error arises from miscalibration of the relation between measured galaxy shape and inferred shear, arising from inaccurate correction for the circular blurring of galaxy images due to atmospheric seeing. Photometric redshift errors impact shear power spectrum estimates primarily through uncertainties in the scatter and bias of photometric redshift estimates in redshift bins [112, 113]. Any tendency of galaxies to align with their neighbors — or to align with the local mass distribution — can be confused with alignments caused by gravitational lensing, thus biasing dark energy determinations [114, 115]. Finally, uncertainties in the theoretical mass power spectrum on small scales could complicate attempts to use the high-multipole ( $\ell >$  several hundred) shear power spectrum to constrain dark energy. Fortunately, weak lensing surveys should be able to internally constrain the impact of such effects [116].

## DARK ENERGY PROJECTS

A diverse and ambitious set of projects to probe dark energy are in progress or being planned. Here we provide a brief overview of the observational landscape. Table 1 provides a representative sampling, not a comprehensive listing, of projects that are currently proposed or under construction and does not include experiments that have already reported results. All of these projects share the common feature of surveying wide areas to collect large samples of objects — galaxies, clusters, or supernovae.

The Dark Energy Task Force (DETF) report [117] classified dark energy surveys into an approximate sequence: on-going projects, either taking data or soon to be taking

data, are Stage II; near-future, intermediate-scale projects are Stage III; and larger-scale, longer-term future projects are designated Stage IV. More advanced stages are in general expected to deliver tighter dark energy constraints.

## Ground-based surveys

A number of projects are underway to detect clusters and probe dark energy using the Sunyaev-Zel'dovich effect. These surveys are coordinated with optical surveys that can determine cluster redshifts. The Atacama Pathfinder EXperiment (APEX) survey in Chile will cover up to 1000 square degrees. The largest of these projects are the Atacama Cosmology Telescope (ACT) and the South Pole Telescope (SPT), the latter of which will carry out a 4,000 square degree survey.

A number of optical imaging surveys are planned or proposed which can study dark energy through weak lensing, clusters, and angular BAO using a single wide-area survey. These projects use telescopes of intermediate to large aperture and wide field-of-view, gigapixel-scale CCD cameras, and are deployed at the best astronomical sites in order to obtain deep galaxy photometry and shape measurements. They deliver photometric-redshift information through color measurements using multiple passbands. The ESO VLT Survey Telescope (VST) on Cerro Paranal will carry out public surveys, including the 1500 sq. deg. KIDS survey and a shallower, 5000 sq. deg. survey (ATLAS). The Panoramic Survey Telescope and Rapid Response System (Pan-STARRS)-1 uses a 1.8-m wide-field telescope to carry out several wide-area surveys from Haleakala; in the future, they hope to deploy  $4 \times 1.8$ -m telescopes at Mauna Kea in Pan-STARRS-4. The Dark Energy Survey (DES) will use a new 3 sq. deg. imager with red-sensitive CCDs on a 4-m telescope at Cerro Tololo Inter-American Observatory (CTIO) in Chile to carry out a 5,000 sq. deg. survey in 5 optical passbands, covering the same survey area as the SPT and partnering with the ESO VISTA Hemisphere Survey which will survey the same area in 3 near-infrared bands. Hyper Suprime-Cam is a new wide-field imager planned for the Subaru telescope on Mauna Kea that will be used to carry out a deep survey over 2000 sq. deg. The Advanced Liquid-mirror Probe of Asteroids, Cosmology and Astrophysics (ALPACA) is a proposed rotating liquid mercury telescope that would repeatedly survey a long, narrow strip of the sky at CTIO. The most ambitious of these projects is the Large Synoptic Survey Telescope (LSST), which would deploy a multi-Gigapixel camera with 10 sq. deg. field-of-view on a new telescope on Cerro Pachon in Chile to survey 15,000 sq. deg. over 10 years.

Several large spectroscopic surveys have been designed to detect baryon acoustic oscillations by measuring  $\sim 10^5 - 10^9$  galaxy and QSO redshifts using large multi-fiber spectrographs. WiggleZ is using the Anglo-Australian Telescope to collect spectra of 400,000 galaxies in the redshift range  $0.5 < z < 1$ . The Baryon Oscillation Sky Survey (BOSS) will use the SDSS telescope in New Mexico to measure galaxy spectra out to  $z \sim 0.6$ . The Hobby Eberly Telescope Dark energy EXperiment (HETDEX) plans to target Ly- $\alpha$  emitters at higher redshift,  $2 < z < 4$ . The Wide-Field Multi-Object Spectrograph (WFMOS), proposed for the Subaru telescope, would target galaxies at  $z < 1.3$  and Lyman-break galaxies at  $2.5 < z < 3.5$ . The Physics of the Accelerating

**TABLE 1.** Dark energy projects proposed or under construction. Stage refers to the DETF time-scale classification.

Survey	Description	Probes	Stage
Ground-based:			
ACT	SZE, 6-m	CL	II
APEX	SZE, 12-m	CL	II
SPT	SZE, 10-m	CL	II
VST	Optical imaging, 2.6-m	BAO,CL,WL	II
Pan-STARRS 1(4)	Optical imaging, 1.8-m( $\times 4$ )	All	II(III)
DES	Optical imaging, 4-m	All	III
Hyper Suprime-Cam	Optical imaging, 8-m	WL,CL,BAO	III
ALPACA	Optical imaging, 8-m	SN, BAO, CL	III
LSST	Optical imaging, 6.8-m	All	IV
AAT WiggleZ	Spectroscopy, 4-m	BAO	II
HETDEX	Spectroscopy, 9.2-m	BAO	III
PAU	Multi-filter imaging, 2-3-m	BAO	III
SDSS BOSS	Spectroscopy, 2.5-m	BAO	III
WFMOs	Spectroscopy, 8-m	BAO	III
HSHS	21-cm radio telescope	BAO	III
SKA	km <sup>2</sup> radio telescope	BAO, WL	IV
Space-based:			
<i>JDEM Candidates</i>			
ADEPT	Spectroscopy	BAO, SN	IV
DESTINY	Grism spectrophotometry	SN	IV
SNAP	Optical+NIR+spectro	All	IV
<i>Proposed ESA Missions</i>			
Euclid	Imaging & spectroscopy	WL, BAO, CL	
eROSITA	X-ray	CL	
<i>CMB Space Probe</i>			
Planck	SZE	CL	
<i>Beyond Einstein Probe</i>			
Constellation-X	X-ray	CL	IV

Universe (PAU) is a Spanish project to deploy a wide-field camera with a large number of narrow filters to measure coarse-grained galaxy spectra out to  $z = 0.9$ .

Finally, the proposed Square Kilometer Array (SKA), an array of radio antennas with unprecedented collecting area, would probe dark energy using baryon acoustic oscillations and weak lensing of galaxies via measurements of the 21-cm line signature of neutral hydrogen (HI). The Hubble Sphere Hydrogen Survey (HSHS) aims to carry out a 21-cm BAO survey on a shorter timescale.

## Space-based surveys

Three of the proposed space projects are candidates for the Joint Dark Energy Mission (JDEM), a joint mission of the U.S. Department of Energy (DOE) and the NASA Be-

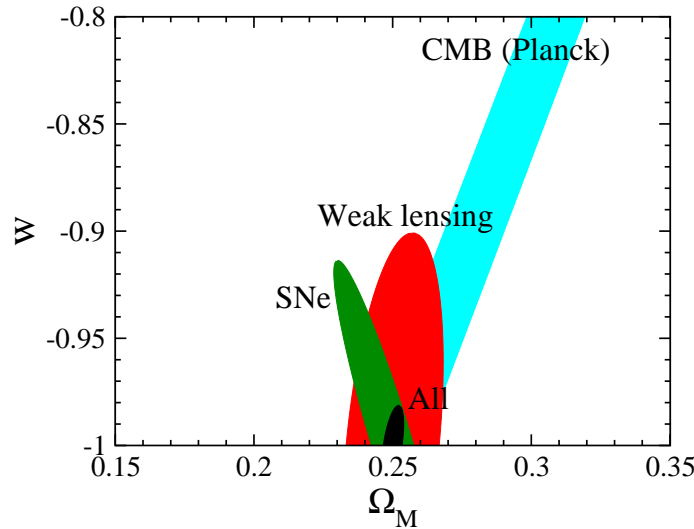


**FIGURE 11.** Illustration of forecast constraints on dark energy parameters. Shown are 68% C.L. uncertainties in the  $\Omega_m$  vs.  $w$  plane, for one version of the proposed SNAP experiment, which combines a narrow-area survey of 2000 SNe to  $z = 1.7$  and a weak lensing survey of 1000 sq. deg. From Frieman et al. [13].

yond Einstein program, targeted at dark energy science. SuperNova/Acceleration Probe (SNAP) proposes to study dark energy using a dedicated 2-m class telescope. With imaging in 9 optical and near-infrared passbands and follow-up spectroscopy of supernovae, it is principally designed to probe SNe Ia and weak lensing, taking advantage of the excellent optical image quality and near-infrared transparency of a space-based platform. Fig. 11 gives an illustration of the statistical constraints that the proposed SNAP mission could achieve, by combining SN and weak lensing observations with results from the Planck CMB mission. The Dark Energy Space Telescope (DESTINY) would use a similar-size telescope with a near-infrared grism spectrograph to study supernovae. The Advanced Dark Energy Physics Telescope (ADEPT) is a spectroscopic mission with the primary goal of constraining dark energy via baryon acoustic oscillations at  $z \sim 2$  as well as supernovae. Another proposed mission within the NASA Beyond Einstein program is Constellation-X, which could observe X-ray clusters with unprecedented sensitivity.

There is one European Space Agency (ESA) mission nearing launch and two concepts under study. The Planck mission, planned for launch in early 2009, in addition to pinning down other cosmological parameters important for dark energy, will detect thousands of galaxy clusters using the SZE. Dark Universe Explorer (DUNE) and SPACE are optical missions to study dark energy using weak lensing and baryon acoustic oscillations, respectively, that have recently been combined into a single concept mission known as Euclid. Finally, the extended ROentgen Survey with an Imaging Telescope Array (eROSITA), a German-Russian collaboration, is a planned X-ray telescope that will study dark energy using the abundance of X-ray clusters.

## CONCLUSION

The case for an accelerating Universe, which began with the supernova discoveries ten years ago, has strengthened into a compelling web of evidence in the years since. The simplest explanation for acceleration is dark energy, and the simplest candidate for dark energy is vacuum energy—the cosmological constant. However, given the lack of understanding of the cosmological constant problem, the relative dearth of well-motivated models, and the fact that the Universe likely underwent a previous epoch of accelerated expansion (primordial inflation), it is best to keep an open mind and rely on experiment as a guide to illuminating the underlying cause. Probing the history of cosmic expansion and of the growth of structure offers the best hope of pointing us down the correct path. An impressive array of experiments with that aim are underway or planned, exploiting four primary, complementary techniques of probing cosmic acceleration: supernovae, baryon acoustic oscillations, clusters, and weak lensing. Exploiting the complementarity of these multiple probes will be key, since we do not know what the ultimate systematic error floors for each method will be. Ten to fifteen years from now, we should know whether the effective dark energy equation of state parameter is consistent with vacuum energy, that is,  $w = -1$ , to within a few percent, or not. The Chinese origin of the phrase “may you live in interesting times” is apparently unsubstantiated. Let us hope that also calls into doubt the third part of the same proverb, “may you find what you are looking for”, since the alternative would certainly be more interesting.

## ACKNOWLEDGMENTS

I would like to thank the organizers of the course, especially Jailson Alcaniz, Paulo Pellegrini, and Eduardo Telles, along with all the participants, for an enjoyable week and a stimulating atmosphere at the Observatorio in Rio. I thank Michael Turner and Dragan Huterer for collaborative effort on our dark energy review, which helped in the preparation of the lectures and of these lecture notes. Research supported by the U.S. Department of Energy at Fermilab and at the University of Chicago and by the Kavli Institute for Cosmological Physics at Chicago, an NSF Physics Frontier Center.

## REFERENCES

1. A. G. Riess, A. V. Filippenko, P. Challis, A. Clocchiatti, A. Diercks, P. M. Garnavich, R. L. Gilliland, C. J. Hogan, S. Jha, R. P. Kirshner, B. Leibundgut, M. M. Phillips, D. Reiss, B. P. Schmidt, R. A. Schommer, R. C. Smith, J. Spyromilio, C. Stubbs, N. B. Suntzeff, and J. Tonry, *AJ* **116**, 1009–1038 (1998), [arXiv:astro-ph/9805201](#).
2. S. Perlmutter, G. Aldering, G. Goldhaber, R. A. Knop, P. Nugent, P. G. Castro, S. Deustua, S. Fabbro, A. Goobar, D. E. Groom, I. M. Hook, A. G. Kim, M. Y. Kim, J. C. Lee, N. J. Nunes, R. Pain, C. R. Pennypacker, R. Quimby, C. Lidman, R. S. Ellis, M. Irwin, R. G. McMahon, P. Ruiz-Lapuente, N. Walton, B. Schaefer, B. J. Boyle, A. V. Filippenko, T. Matheson, A. S. Fruchter, N. Panagia, H. J. M. Newberg, W. J. Couch, and The Supernova Cosmology Project, *ApJ* **517**, 565–586 (1999), [arXiv:astro-ph/9812133](#).

3. E. J. Copeland, M. Sami, and S. Tsujikawa, *Int. J. Mod. Phys. D* **15**, 1753–1936 (2006), hep-th/0603057.
4. T. Padmanabhan, *Phys. Rept.* **380**, 235–320 (2003), hep-th/0212290.
5. P. J. E. Peebles, and B. Ratra, *Rev. Mod. Phys.* **75**, 559–606 (2003), astro-ph/0207347.
6. J.-P. Uzan, *Gen. Rel. Grav.* **39**, 307–342 (2007), astro-ph/0605313.
7. D. Huterer, and M. S. Turner, *Phys. Rev.* **D64**, 123527 (2001), astro-ph/0012510.
8. V. Sahni, and A. Starobinsky, *astro-ph/0610026* (2006), astro-ph/0610026.
9. E. V. Linder, *astro-ph/0704.2064* (2007), arXiv:0704.2064[astro-ph].
10. S. M. Carroll, W. H. Press, and E. L. Turner, *ARAAS* **30**, 499–542 (1992).
11. S. M. Carroll, *Living Rev. Rel.* **4**, 1 (2001), astro-ph/0004075.
12. S. Weinberg, *Rev. Mod. Phys.* **61**, 1–23 (1989).
13. J. Frieman, M. Turner, and D. Huterer, *ArXiv e-prints* **803** (2008), 0803.0982.
14. S. Dodelson, *Modern cosmology*, Amsterdam (Netherlands): Academic Press, 2003.
15. E. W. Kolb, and M. S. Turner, *The early universe*, Reading, MA: Addison-Wesley, 1990.
16. J. A. Peacock, *Cosmological Physics*, Cambridge, UK: Cambridge University Press, 1999.
17. P. J. E. Peebles, *Principles of physical cosmology*, Princeton, NJ: Princeton University Press, 1993.
18. W. L. Freedman, B. F. Madore, B. K. Gibson, L. Ferrarese, D. D. Kelson, S. Sakai, J. R. Mould, R. C. Kennicutt, Jr., H. C. Ford, J. A. Graham, J. P. Huchra, S. M. G. Hughes, G. D. Illingworth, L. M. Macri, and P. B. Stetson, *ApJ* **553**, 47–72 (2001), arXiv:astro-ph/0012376.
19. Y. B. Zel’dovich, *Sov. Phys. Usp.* **11**, 381–393 (1968).
20. A. H. Guth, *Phys. Rev.* **D23**, 347–356 (1981).
21. G. Efstathiou, W. J. Sutherland, and S. J. Maddox, *Nature* **348**, 705–707 (1990).
22. J. A. Frieman, C. T. Hill, A. Stebbins, and I. Waga, *Phys. Rev. Lett.* **75**, 2077–2080 (1995), astro-ph/9505060.
23. L. M. Krauss, and M. S. Turner, *Gen. Rel. Grav.* **27**, 1137–1144 (1995), astro-ph/9504003.
24. J. P. Ostriker, and P. J. Steinhardt, *Nature* **377**, 600–602 (1995).
25. W. Hillebrandt, and J. C. Niemeyer, *ARAAS* **38**, 191–230 (2000), arXiv:astro-ph/0006305.
26. W. D. Arnett, *ApJ* **253**, 785–797 (1982).
27. P. Hoefflich, *astro-ph/0409170* (2004).
28. T. Plewa, A. C. Calder, and D. Q. Lamb, *ApJ* **612**, L37–L40 (2004), arXiv:astro-ph/0405163.
29. M. M. Phillips, *ApJ* **413**, L105–L108 (1993).
30. A. G. Riess, *PASP* **112**, 1284 (2000), arXiv:astro-ph/0005229.
31. S. Perlmutter, and B. P. Schmidt, “Measuring Cosmology with Supernovae,” in *Supernovae and Gamma-Ray Bursters*, edited by K. Weiler, 2003, vol. 598 of *Lecture Notes in Physics*, Berlin Springer Verlag, pp. 195–217.
32. J. Dunkley, E. Komatsu, M. R. Nolta, D. N. Spergel, D. Larson, G. Hinshaw, L. Page, C. L. Bennett, B. Gold, N. Jarosik, J. L. Weiland, M. Halpern, R. S. Hill, A. Kogut, M. Limon, S. S. Meyer, G. S. Tucker, E. Wollack, and E. L. Wright, *ArXiv e-prints* **803** (2008), 0803.0586.
33. A. H. Jaffe, P. A. Ade, A. Balbi, J. J. Bock, J. R. Bond, J. Borrill, A. Boscaleri, K. Coble, B. P. Crill, P. de Bernardis, P. Farese, P. G. Ferreira, K. Ganga, M. Giacometti, S. Hanany, E. Hivon, V. V. Hristov, A. Iacoangeli, A. E. Lange, A. T. Lee, L. Martinis, S. Masi, P. D. Mauskopf, A. Melchiorri, T. Montroy, C. B. Netterfield, S. Oh, E. Pascale, F. Piacentini, D. Pogosyan, S. Prunet, B. Rabbii, S. Rao, P. L. Richards, G. Romeo, J. E. Ruhl, F. Scaramuzzi, D. Sforna, G. F. Smoot, R. Stompor, C. D. Winant, and J. H. Wu, *Physical Review Letters* **86**, 3475–3479 (2001), arXiv:astro-ph/0007333.
34. C. Pryke, N. W. Halverson, E. M. Leitch, J. Kovac, J. E. Carlstrom, W. L. Holzapfel, and M. Drago- van, *ApJ* **568**, 46–51 (2002), arXiv:astro-ph/0104490.
35. S. Hanany, P. Ade, A. Balbi, J. Bock, J. Borrill, A. Boscaleri, P. de Bernardis, P. G. Ferreira, V. V. Hristov, A. H. Jaffe, A. E. Lange, A. T. Lee, P. D. Mauskopf, C. B. Netterfield, S. Oh, E. Pascale, B. Rabbii, P. L. Richards, G. F. Smoot, R. Stompor, C. D. Winant, and J. H. P. Wu, *ApJ* **545**, L5–L9 (2000), arXiv:astro-ph/0005123.
36. E. Komatsu, J. Dunkley, M. R. Nolta, C. L. Bennett, B. Gold, G. Hinshaw, N. Jarosik, D. Larson, M. Limon, L. Page, D. N. Spergel, M. Halpern, R. S. Hill, A. Kogut, S. S. Meyer, G. S. Tucker, J. L. Weiland, E. Wollack, and E. L. Wright, *ArXiv e-prints* **803** (2008), 0803.0547.
37. D. J. Eisenstein, I. Zehavi, D. W. Hogg, R. Scoccimarro, M. R. Blanton, R. C. Nichol, R. Scranton,



- H.-J. Seo, M. Tegmark, Z. Zheng, S. F. Anderson, J. Annis, N. Bahcall, J. Brinkmann, S. Burles, F. J. Castander, A. Connolly, I. Csabai, M. Doi, M. Fukugita, J. A. Frieman, K. Glazebrook, J. E. Gunn, J. S. Hendry, G. Hennessy, Z. Ivezić, S. Kent, G. R. Knapp, H. Lin, Y.-S. Loh, R. H. Lupton, B. Margon, T. A. McKay, A. Meiksin, J. A. Munn, A. Pope, M. W. Richmond, D. Schlegel, D. P. Schneider, K. Shimasaku, C. Stoughton, M. A. Strauss, M. SubbaRao, A. S. Szalay, I. Szapudi, D. L. Tucker, B. Yanny, and D. G. York, *ApJ* **633**, 560–574 (2005), [arXiv:astro-ph/0501171](#).
38. W. J. Percival, S. Cole, D. J. Eisenstein, R. C. Nichol, J. A. Peacock, A. C. Pope, and A. S. Szalay, *MNRAS* **381**, 1053–1066 (2007), [arXiv:0705.3323](#).
39. M. Tegmark, D. J. Eisenstein, M. A. Strauss, D. H. Weinberg, M. R. Blanton, J. A. Frieman, M. Fukugita, J. E. Gunn, A. J. S. Hamilton, G. R. Knapp, R. C. Nichol, J. P. Ostriker, N. Padmanabhan, W. J. Percival, D. J. Schlegel, D. P. Schneider, R. Scoccimarro, U. Seljak, H.-J. Seo, M. Swanson, A. S. Szalay, M. S. Vogele, J. Yoo, I. Zehavi, K. Abazajian, S. F. Anderson, J. Annis, N. A. Bahcall, B. Bassett, A. Berlind, J. Brinkmann, T. Budavari, F. Castander, A. Connolly, I. Csabai, M. Doi, D. P. Finkbeiner, B. Gillespie, K. Glazebrook, G. S. Hennessy, D. W. Hogg, Ž. Ivezić, B. Jain, D. Johnston, S. Kent, D. Q. Lamb, B. C. Lee, H. Lin, J. Loveday, R. H. Lupton, J. A. Munn, K. Pan, C. Park, J. Peoples, J. R. Pier, A. Pope, M. Richmond, C. Rockosi, R. Scranton, R. K. Sheth, A. Stebbins, C. Stoughton, I. Szapudi, D. L. Tucker, D. E. V. Berk, B. Yanny, and D. G. York, *Phys. Rev. D* **74**, 123507 (2006), [arXiv:astro-ph/0608632](#).
40. M. Kowalski, D. Rubin, G. Aldering, R. J. Agostinho, A. Amadon, R. Amanullah, C. Balland, K. Barbary, G. Blanc, P. J. Challis, A. Conley, N. V. Connolly, R. Covarrubias, K. S. Dawson, S. E. Deustua, R. Ellis, S. Fabbro, V. Fadeyev, X. Fan, B. Farris, G. Folatelli, B. L. Frye, G. Garavini, E. L. Gates, L. Germany, G. Goldhaber, B. Goldman, A. Goobar, D. E. Groom, J. Haussinski, D. Hardin, I. Hook, S. Kent, A. G. Kim, R. A. Knop, C. Lidman, E. V. Linder, J. Mendez, J. Meyers, G. J. Miller, M. Moniez, A. M. Mourao, H. Newberg, S. Nobili, P. E. Nugent, R. Pain, O. Perdureau, S. Perlmutter, M. M. Phillips, V. Prasad, R. Quimby, N. Regnault, J. Rich, E. P. Rubenstein, P. Ruiz-Lapuente, F. D. Santos, B. E. Schaefer, R. A. Schommer, R. C. Smith, A. M. Soderberg, A. L. Spadafora, L. Strolger, M. Strovink, N. B. Suntzeff, N. Suzuki, R. C. Thomas, N. A. Walton, L. Wang, W. M. Wood-Vasey, and J. L. Yun, *ArXiv e-prints* **804** (2008), [0804.4142](#).
41. P. S. Drell, T. J. Loredo, and I. Wasserman, *ApJ* **530**, 593–617 (2000), [arXiv:astro-ph/9905027](#).
42. A. N. Aguirre, *ApJ* **512**, L19–L22 (1999), [arXiv:astro-ph/9811316](#).
43. R. A. Knop, G. Aldering, R. Amanullah, P. Astier, G. Blanc, M. S. Burns, A. Conley, S. E. Deustua, M. Doi, R. Ellis, S. Fabbro, G. Folatelli, A. S. Fruchter, G. Garavini, S. Garmond, K. Garton, R. Gibbons, G. Goldhaber, A. Goobar, D. E. Groom, D. Hardin, I. Hook, D. A. Howell, A. G. Kim, B. C. Lee, C. Lidman, J. Mendez, S. Nobili, P. E. Nugent, R. Pain, N. Panagia, C. R. Pennypacker, S. Perlmutter, R. Quimby, J. Raux, N. Regnault, P. Ruiz-Lapuente, G. Sainoin, B. Schaefer, K. Schahmanche, E. Smith, A. L. Spadafora, V. Stanishev, M. Sullivan, N. A. Walton, L. Wang, W. M. Wood-Vasey, and N. Yasuda, *ApJ* **598**, 102–137 (2003), [arXiv:astro-ph/0309368](#).
44. A. G. Riess, P. E. Nugent, R. L. Gilliland, B. P. Schmidt, J. Tonry, M. Dickinson, R. I. Thompson, T. Budavári, S. Casertano, A. S. Evans, A. V. Filippenko, M. Livio, D. B. Sanders, A. E. Shapley, H. Spinrad, C. C. Steidel, D. Stern, J. Surace, and S. Veilleux, *ApJ* **560**, 49–71 (2001), [arXiv:astro-ph/0104455](#).
45. A. G. Riess, L.-G. Strolger, J. Tonry, S. Casertano, H. C. Ferguson, B. Mobasher, P. Challis, A. V. Filippenko, S. Jha, W. Li, R. Chornock, R. P. Kirshner, B. Leibundgut, M. Dickinson, M. Livio, M. Giavalisco, C. C. Steidel, T. Benítez, and Z. Tsvetanov, *ApJ* **607**, 665–687 (2004), [arXiv:astro-ph/0402512](#).
46. A. G. Riess, L.-G. Strolger, S. Casertano, H. C. Ferguson, B. Mobasher, B. Gold, P. J. Challis, A. V. Filippenko, S. Jha, W. Li, J. Tonry, R. Foley, R. P. Kirshner, M. Dickinson, E. MacDonald, D. Eisenstein, M. Livio, J. Younger, C. Xu, T. Dahlén, and D. Stern, *ApJ* **659**, 98–121 (2007), [arXiv:astro-ph/0611572](#).
47. P. Astier, J. Guy, N. Regnault, R. Pain, E. Aubourg, D. Balam, S. Basa, R. G. Carlberg, S. Fabbro, D. Fouchez, I. M. Hook, D. A. Howell, H. Lafoux, J. D. Neill, N. Palanque-Delabrouille, K. Perrett, C. J. Pritchet, J. Rich, M. Sullivan, R. Taillet, G. Aldering, P. Antilogus, V. Arsenijevic, C. Balland, S. Baumont, J. Bronder, H. Courtois, R. S. Ellis, M. Filiol, A. C. Gonçalves, A. Goobar, D. Guide, D. Hardin, V. Lusser, C. Lidman, R. McMahon, M. Mouchet, A. Mourao, S. Perlmutter, P. Ripoché,

- C. Tao, and N. Walton, *A & A* **447**, 31–48 (2006), arXiv:astro-ph/0510447.
48. G. Miknaitis, G. Pignata, A. Rest, W. M. Wood-Vasey, S. Blondin, P. Challis, R. C. Smith, C. W. Stubbs, N. B. Suntzeff, R. J. Foley, T. Matheson, J. L. Tonry, C. Aguilera, J. W. Blackman, A. C. Becker, A. Clocchiatti, R. Covarrubias, T. M. Davis, A. V. Filippenko, A. Garg, P. M. Garnavich, M. Hicken, S. Jha, K. Krisciunas, R. P. Kirshner, B. Leibundgut, W. Li, A. Miceli, G. Narayan, J. L. Prieto, A. G. Riess, M. E. Salvo, B. P. Schmidt, J. Sollerman, J. Spyromilio, and A. Zenteno, *ApJ* **666**, 674–693 (2007), arXiv:astro-ph/0701043.
  49. W. M. Wood-Vasey, G. Miknaitis, C. W. Stubbs, S. Jha, A. G. Riess, P. M. Garnavich, R. P. Kirshner, C. Aguilera, A. C. Becker, J. W. Blackman, S. Blondin, P. Challis, A. Clocchiatti, A. Conley, R. Covarrubias, T. M. Davis, A. V. Filippenko, R. J. Foley, A. Garg, M. Hicken, K. Krisciunas, B. Leibundgut, W. Li, T. Matheson, A. Miceli, G. Narayan, G. Pignata, J. L. Prieto, A. Rest, M. E. Salvo, B. P. Schmidt, R. C. Smith, J. Sollerman, J. Spyromilio, J. L. Tonry, N. B. Suntzeff, and A. Zenteno, *ApJ* **666**, 694–715 (2007), arXiv:astro-ph/0701041.
  50. S. Jha, A. G. Riess, and R. P. Kirshner, *ApJ* **659**, 122–148 (2007), arXiv:astro-ph/0612666.
  51. L. Hui, and P. B. Greene, *Phys. Rev. D* **73**, 123526 (2006), arXiv:astro-ph/0512159.
  52. J. A. Frieman, B. Bassett, A. Becker, C. Choi, D. Cinabro, F. DeJongh, D. L. Depoy, B. Dilday, M. Doi, P. M. Garnavich, C. J. Hogan, J. Holtzman, M. Im, S. Jha, R. Kessler, K. Konishi, H. Lampeitl, J. Marriner, J. L. Marshall, D. McGinnis, G. Miknaitis, R. C. Nichol, J. L. Prieto, A. G. Riess, M. W. Richmond, R. Romani, M. Sako, D. P. Schneider, M. Smith, N. Takanashi, K. Tokita, K. van der Heyden, N. Yasuda, C. Zheng, J. Adelman-McCarthy, J. Annis, R. J. Assef, J. Barentine, R. Bender, R. D. Blandford, W. N. Boroski, M. Bremer, H. Brewington, C. A. Collins, A. Crotts, J. Dembicky, J. Eastman, A. Edge, E. Edmondson, E. Elson, M. E. Eyer, A. V. Filippenko, R. J. Foley, S. Frank, A. Goobar, T. Gueth, J. E. Gunn, M. Harvanek, U. Hopp, Y. Ihara, Ž. Ivezić, S. Kahn, J. Kaplan, S. Kent, W. Ketzbeck, S. J. Kleinman, W. Kollatschny, R. G. Kron, J. Krzysiński, D. Lamenti, G. Leloudas, H. Lin, D. C. Long, J. Lucey, R. H. Lupton, E. Malanushenko, V. Malanushenko, R. J. McMillan, J. Mendez, C. W. Morgan, T. Morokuma, A. Nitta, L. Ostman, K. Pan, C. M. Rockosi, A. K. Romer, P. Ruiz-Lapuente, G. Saurage, K. Schlesinger, S. A. Snedden, J. Sollerman, C. Stoughton, M. Stritzinger, M. Subba Rao, D. Tucker, P. Vaisanen, L. C. Watson, S. Watters, J. C. Wheeler, B. Yanny, and D. York, *AJ* **135**, 338–347 (2008), arXiv:0708.2749.
  53. M. Sako, B. Bassett, A. Becker, D. Cinabro, F. DeJongh, D. L. Depoy, B. Dilday, M. Doi, J. A. Frieman, P. M. Garnavich, C. J. Hogan, J. Holtzman, S. Jha, R. Kessler, K. Konishi, H. Lampeitl, J. Marriner, G. Miknaitis, R. C. Nichol, J. L. Prieto, A. G. Riess, M. W. Richmond, R. Romani, D. P. Schneider, M. Smith, M. Subba Rao, N. Takanashi, K. Tokita, K. van der Heyden, N. Yasuda, C. Zheng, J. Barentine, H. Brewington, C. Choi, J. Dembicky, M. Harnavek, Y. Ihara, M. Im, W. Ketzbeck, S. J. Kleinman, J. Krzysiński, D. C. Long, E. Malanushenko, V. Malanushenko, R. J. McMillan, T. Morokuma, A. Nitta, K. Pan, G. Saurage, and S. A. Snedden, *AJ* **135**, 348–373 (2008), arXiv:0708.2750.
  54. J. Guy, P. Astier, S. Nobili, N. Regnault, and R. Pain, *A & A* **443**, 781–791 (2005), arXiv:astro-ph/0506583.
  55. J. Guy, P. Astier, S. Baumont, D. Hardin, R. Pain, N. Regnault, S. Basa, R. G. Carlberg, A. Conley, S. Fabbro, D. Fouchez, I. M. Hook, D. A. Howell, K. Perrett, C. J. Pritchett, J. Rich, M. Sullivan, P. Antilogus, E. Aubourg, G. Bazin, J. Bronder, M. Filiol, N. Palanque-Delabrouille, P. Ripoche, and V. Ruhlmann-Kleider, *A & A* **466**, 11–21 (2007), arXiv:astro-ph/0701828.
  56. J. A. Frieman, D. Huterer, E. V. Linder, and M. S. Turner, *Phys. Rev. D* **67**, 083505 (2003), arXiv:astro-ph/0208100.
  57. S. Boughn, and R. Crittenden, *Nature* **427**, 45–47 (2004), astro-ph/0305001.
  58. P. Fosalba, and E. Gaztanaga, *Mon. Not. Roy. Astron. Soc.* **350**, L37–L41 (2004), astro-ph/0305468.
  59. N. Afshordi, Y.-S. Loh, and M. A. Strauss, *Phys. Rev. D* **69**, 083524 (2004), astro-ph/0308260.
  60. R. Scranton, A. J. Connolly, R. C. Nichol, A. Stebbins, I. Szapudi, D. J. Eisenstein, N. Afshordi, T. Budavari, I. Csabai, J. A. Frieman, J. E. Gunn, D. Johnson, Y. Loh, R. H. Lupton, C. J. Miller, E. S. Sheldon, R. S. Sheth, A. S. Szalay, M. Tegmark, and Y. Xu, *astro-ph/0307335* (2003), astro-ph/0307335.
  61. P. Schneider, “Part 3: Weak gravitational lensing,” in *Saas-Fee Advanced Course 33: Gravitational Lensing: Strong, Weak and Micro*, edited by G. Meylan, P. Jetzer, P. North, P. Schneider, C. S.

- Kochanek, and J. Wambsganss, 2006, pp. 269–451.
62. D. Munshi, P. Valageas, L. Van Waerbeke, and A. Heavens, *astro-ph/0612667* (2006), [astro-ph/0612667](#).
  63. D. J. Bacon, A. R. Refregier, and R. S. Ellis, *MNRAS* **318**, 625–640 (2000), [arXiv:astro-ph/0003008](#).
  64. N. Kaiser, G. Wilson, and G. A. Luppino, *astro-ph/0003338* (2000), [astro-ph/0003338](#).
  65. L. Van Waerbeke, Y. Mellier, T. Erben, J. C. Cuillandre, F. Bernardeau, R. Maoli, E. Bertin, H. J. Mc Cracken, O. Le Fèvre, B. Fort, M. Dantel-Fort, B. Jain, and P. Schneider, *A & A* **358**, 30–44 (2000), [arXiv:astro-ph/0002500](#).
  66. D. M. Wittman, J. A. Tyson, D. Kirkman, I. Dell’Antonio, and G. Bernstein, *Nature* **405**, 143–148 (2000), [arXiv:astro-ph/0003014](#).
  67. M. Jarvis, B. Jain, G. Bernstein, and D. Dolney, *ApJ* **644**, 71–79 (2006), [astro-ph/0502243](#).
  68. H. Hoekstra, Y. Mellier, L. van Waerbeke, E. Semboloni, L. Fu, M. J. Hudson, L. C. Parker, I. Tereno, and K. Benabed, *ApJ* **647**, 116–127 (2006), [arXiv:astro-ph/0511089](#).
  69. R. Massey, J. Rhodes, R. Ellis, N. Scoville, A. Leauthaud, A. Finoguenov, P. Capak, D. Bacon, H. Aussel, J.-P. Kneib, A. Koekemoer, H. McCracken, B. Mobasher, S. Pires, A. Refregier, S. Sasaki, J.-L. Starck, Y. Taniguchi, A. Taylor, and J. Taylor, *Nature* **445**, 286–290 (2007), [arXiv:astro-ph/0701594](#).
  70. D. Huterer, *Phys. Rev. D* **65**, 063001 (2002), [astro-ph/0106399](#).
  71. W. Hu, *Phys. Rev. D* **65**, 023003 (2002), [arXiv:astro-ph/0108090](#).
  72. S. W. Allen, R. W. Schmidt, H. Ebeling, A. C. Fabian, and L. van Speybroeck, *Mon. Not. Roy. Astron. Soc.* **353**, 457 (2004), [astro-ph/0405340](#).
  73. S. W. Allen, D. A. Rapetti, R. W. Schmidt, H. Ebeling, G. Morris, and A. C. Fabian, *astro-ph/0706.0033* (2007), [0706.0033](#).
  74. M. Fukugita, T. Futamase, M. Kasai, and E. L. Turner, *ApJ* **393**, 3–21 (1992).
  75. C. S. Kochanek, *ApJ* **466**, 638 (1996), [arXiv:astro-ph/9510077](#).
  76. J. L. Mitchell, C. R. Keeton, J. A. Frieman, and R. K. Sheth, *ApJ* **622**, 81–98 (2005), [arXiv:astro-ph/0401138](#).
  77. M. Oguri, N. Inada, M. A. Strauss, C. S. Kochanek, G. T. Richards, D. P. Schneider, R. H. Becker, M. Fukugita, M. D. Gregg, P. B. Hall, J. F. Hennawi, D. E. Johnston, I. Kayo, C. R. Keeton, B. Pindor, M.-S. Shin, E. L. Turner, R. L. White, D. G. York, S. F. Anderson, N. A. Bahcall, R. J. Brunner, S. Burles, F. J. Castander, K. Chiu, A. Clocchiatti, D. Eisenstein, J. A. Frieman, Y. Kawano, R. Lupton, T. Morokuma, H.-W. Rix, R. Scranton, and E. S. Sheldon, *ArXiv:astro-ph/0708.0825* (2007), [0708.0825](#).
  78. K.-H. Chae, *ApJ* **658**, L71–L74 (2007), [arXiv:astro-ph/0611898](#).
  79. S. Weinberg, *Phys. Rev. Lett.* **59**, 2607 (1987).
  80. R. Bousso, and J. Polchinski, *JHEP* **06**, 006 (2000), [hep-th/0004134](#).
  81. L. Susskind, *hep-th/0302219* (2003), [hep-th/0302219](#).
  82. B. Ratra, and P. J. E. Peebles, *Phys. Rev. D* **37**, 3406 (1988).
  83. C. Wetterich, *Nucl. Phys.* **B302**, 668 (1988).
  84. I. Zlatev, L.-M. Wang, and P. J. Steinhardt, *Phys. Rev. Lett.* **82**, 896–899 (1999), [astro-ph/9807002](#).
  85. K. Coble, S. Dodelson, and J. A. Frieman, *Phys. Rev. D* **55**, 1851–1859 (1997), [astro-ph/9608122](#).
  86. Y. Nomura, T. Watari, and T. Yanagida, *Phys. Rev. D* **61**, 105007+ (2000), [arXiv:hep-ph/9911324](#).
  87. L. J. Hall, Y. Nomura, and S. J. Oliver, *Phys. Rev. Lett.* **95**, 141302 (2005), [astro-ph/0503706](#).
  88. R. R. Caldwell, and E. V. Linder, *Phys. Rev. Lett.* **95**, 141301 (2005), [astro-ph/0505494](#).
  89. G. R. Dvali, G. Gabadadze, and M. Porrati, *Phys. Lett.* **B485**, 208–214 (2000), [hep-th/0005016](#).
  90. C. Deffayet, *Phys. Lett.* **B502**, 199–208 (2001), [hep-th/0010186](#).
  91. S. M. Carroll, V. Duvvuri, M. Trodden, and M. S. Turner, *Phys. Rev. D* **70**, 043528 (2004), [astro-ph/0306438](#).
  92. Y.-S. Song, W. Hu, and I. Sawicki, *Phys. Rev. D* **75**, 044004 (2007), [astro-ph/0610532](#).
  93. R. Gregory, N. Kaloper, R. C. Myers, and A. Padilla, *JHEP* **10**, 069 (2007), [arXiv:0707.2666\[hep-th\]](#).

94. E. W. Kolb, S. Matarrese, and A. Riotto, *New J. Phys.* **8**, 322 (2006), astro-ph/0506534.
95. K. Tomita, *Mon. Not. Roy. Astron. Soc.* **326**, 287 (2001), astro-ph/0011484.
96. H. Alnes, M. Amarzguioui, and O. Gron, *Phys. Rev.* **D73**, 083519 (2006), astro-ph/0512006.
97. K. Enqvist, *astro-ph/0709.2044* (2007), arXiv:0709.2044 [astro-ph].
98. R. R. Caldwell, and A. Stebbins, *Physical Review Letters* **100**, 191302+ (2008), arXiv:0711.3459.
99. M. S. Warren, K. Abazajian, D. E. Holz, and L. Teodoro, *ApJ* **646**, 881–885 (2006), arXiv:astro-ph/0506395.
100. J. L. Tinker, A. V. Kravtsov, A. Klypin, K. Abazajian, M. S. Warren, G. Yepes, S. Gottlober, and D. E. Holz, *ArXiv e-prints* **803** (2008), 0803.2706.
101. L. Wang, and P. J. Steinhardt, *ApJ* **508**, 483–490 (1998), arXiv:astro-ph/9804015.
102. Z. Haiman, J. J. Mohr, and G. P. Holder, *ApJ* **553**, 545–561 (2001), arXiv:astro-ph/0002336.
103. S. Borgani, *astro-ph/0605575* (2006), astro-ph/0605575.
104. J. J. Mohr, “Cluster Survey Studies of the Dark Energy,” in *Observing Dark Energy*, edited by S. C. Wolff, and T. R. Lauer, 2005, vol. 339 of *Astronomical Society of the Pacific Conference Series*, p. 140.
105. S. Majumdar, and J. J. Mohr, *ApJ* **613**, 41–50 (2004), arXiv:astro-ph/0305341.
106. M. Lima, and W. Hu, *Phys. Rev. D* **70**, 043504 (2004), arXiv:astro-ph/0401559.
107. N. Kaiser, *ApJ* **388**, 272–286 (1992).
108. W. Hu, and B. Jain, *Phys. Rev. D* **70**, 043009 (2004), arXiv:astro-ph/0312395.
109. B. Jain, and A. Taylor, *Phys. Rev. Lett.* **91**, 141302 (2003), arXiv:astro-ph/0306046.
110. G. M. Bernstein, and B. Jain, *ApJ* **600**, 17–25 (2004), astro-ph/0309332.
111. M. Takada, and B. Jain, *Mon. Not. Roy. Astron. Soc.* **348**, 897 (2004), astro-ph/0310125.
112. D. Huterer, M. Takada, G. Bernstein, and B. Jain, *MNRAS* **366**, 101–114 (2006), arXiv:astro-ph/0506030.
113. Z. Ma, W. Hu, and D. Huterer, *ApJ* **636**, 21–29 (2006), arXiv:astro-ph/0506614.
114. C. M. Hirata, and U. Seljak, *Phys. Rev. D* **70**, 063526 (2004), arXiv:astro-ph/0406275.
115. C. Heymans, M. White, A. Heavens, C. Vale, and L. van Waerbeke, *MNRAS* **371**, 750–760 (2006), arXiv:astro-ph/0604001.
116. A. R. Zentner, D. H. Rudd, and W. Hu, *astro-ph/0709.4029* (2007), 0709.4029.
117. A. Albrecht, G. Bernstein, R. Cahn, W. L. Freedman, J. Hewitt, W. Hu, J. Huth, M. Kamionkowski, E. W. Kolb, L. Knox, J. C. Mather, S. Staggs, and N. B. Suntzeff, *astro-ph/0609591* (2006).